A Fusarium graminearum effector protein subverts plant immunity by targeting the TaRPM1–TaHSA32 regulatory axis

Yuan Chen

yuan.chen@pku-iaas.edu.cn

Peking University Institute of Advanced Agricultural Sciences

Qunqing Wang

Shandong agricultural university https://orcid.org/0000-0002-3424-8018

Yiman Wan

Peking University Institute of Advanced Agricultural Sciences

Xiaohui Li

Peking University Institute of Advanced Agricultural Sciences

Chunxue Xie

Peking University Institute of Advanced Agricultural Sciences

Zhen Wang

Peking University Institute of Advanced Agricultural Sciences

Liqiang Yao

Peking University Institute of Advanced Agricultural Sciences

Fuqiang Zhu

Peking University Institute of Advanced Agricultural Sciences

Lanxi Zhang

Peking University Institute of Advanced Agricultural Sciences

Qiangqiang Zhang

Peking University Institute of Advanced Agricultural Sciences

Yelin Shan

State Key Laboratory of Wheat Improvement, Peking University Institute of Advanced Agricultural Sciences, Shandong Laboratory of Advanced Agriculture Sciences in Weifang, Shandong 261325, China

Yanyan Liang

State Key Laboratory of Wheat Improvement, Peking University Institute of Advanced Agricultural Sciences, Shandong Laboratory of Advanced Agriculture Sciences in Weifang, Shandong 261325, China

Jianxin Qin

Peking University Institute of Advanced Agricultural Sciences

Jiajie Wu

Shandong Agricultural University https://orcid.org/0000-0002-1536-2421

Zhaomei Qi

Shandong Agricultural University

Article

Keywords: usarium graminearum, wheat, NLR immune receptor, heat-stress-associated 32-kD protein, plant immunity, pathogen effector

Posted Date: January 7th, 2026

DOI: https://doi.org/10.21203/rs.3.rs-8477788/v1

Additional Declarations: There is **NO** Competing Interest.

A *Fusarium graminearum* effector protein subverts plant immunity by targeting the TaRPM1–TaHSA32 regulatory axis

Authors and Affiliations

Yiman Wan[1,2#], Xiaohui Li[1,3], Chunxue Xie[1,4], Zhen Wang[1], Liqiang Yao[1], Fuqiang Zhu[1,5], Lanxi Zhang[1,2], Qiangqiang Zhang[1], Yelin Shan[1,6], Yanyan Liang[1], Jianxin Qin[1], Jiajie Wu[4], Zhaomei Qi[2], Qunqing Wang[2*], Yuan Chen[1*]

1. State Key Laboratory of Wheat Improvement, Peking University Institute of Advanced Agricultural Sciences, Shandong Laboratory of Advanced Agricultural Sciences in Weifang, Weifang, Shandong 261325, China

2. College of Plant Protection, Shandong Agricultural University, Tai'an, Shandong 271018, China

3. College of Life Sciences, National Key Laboratory of Crop Improvement for Stress Tolerance and Production, Northwest Agriculture and Forestry University, Yangling, Shanxi 712100, China

4. State Key Laboratory of Wheat Improvement, College of Agronomy, Shandong Agricultural University, Tai'an, Shandong 271018, China

5. State Key Laboratory of Wheat Improvement, College of Life Sciences, Shandong Agricultural University, Tai'an, Shandong 271018, China

6. Chinese Education Ministry's Key Laboratory of Western Resources and Modern Biotechnology, Key Laboratory of Biotechnology Shaanxi Province, College of Life Sciences, Northwest University, Xi'an 710069, China

*Correspondence: wangqunqing@163.com; yuan.chen@pku-iaas.edu.cn

Abstract

Fusarium graminearum is a devastating wheat pathogen that suppresses host immunity to promote infection. Here, we show that the secreted effector *FgUP7* contributes to pathogen virulence by targeting the NLR immune receptor TaRPM1. TaRPM1 positively regulates wheat resistance to *F. graminearum*. By binding the coiled-coil domain, FgUP7

interferes with early NLR oligomerization and promotes TaRPM1 destabilization. In contrast, the heat-induced co-chaperone TaHSA32 associates with TaRPM1 to stabilize the receptor and prime NLR complexes for activation under fluctuating temperatures. Competitive displacement of TaHSA32 by FgUP7 removes this protective layer, rendering TaRPM1 vulnerable to degradation and thereby diminishing host immune surveillance. This antagonistic interplay provides a mechanistic framework explaining how elevated temperature and pathogen effectors synergistically compromise plant immunity. Notably, transgenic manipulation of TaHSA32 or TaRPM1 does not affect major agronomic traits, highlighting the potential for targeted improvement of resistance. Furthermore, the RPM1–HSA32 regulatory axis is functionally conserved in the model grass *Brachypodium distachyon*, suggesting evolutionary conservation across monocots.

Key words: *Fusarium graminearum*, wheat, NLR immune receptor, heat-stress-associated 32-kD protein, plant immunity, pathogen effector

Introduction

Fusarium head blight (FHB), caused primarily by *Fusarium graminearum*, is a major threat to global wheat production and food security[1]. Disease outbreaks are strongly promoted by high humidity and elevated temperatures during the wheat flowering stage[2,3]. Under these conditions, spike tissues face the combined challenge of environmental stress and pathogen pressure, creating a physiological bottleneck for effective disease resistance. Understanding how wheat integrates thermal stress responses with immune activation is therefore critical, particularly in the context of increasingly frequent heat–humidity events associated with climate change.

F. graminearum is a hemibiotrophic fungus that spreads through the rachis, causing blight of the entire wheat head[4]. Warmer temperatures markedly accelerate its biological processes: mycelial growth, ascospore germination, spike colonization, and toxin production all reach their optimum around 25–30 °C, with accumulation of the trichothecene mycotoxin deoxynivalenol (DON) peaking near 30 °C. Consequently, elevated temperatures not only compromise host immunity but also create highly favorable conditions for fungal proliferation and mycotoxin biosynthesis[5–7]. *F. graminearum* uses a diverse set of intracellular virulence factors to establish infection,

including regulators of transcription, signaling, primary metabolism, and DON biosynthesis[8,9]. In addition, it secretes apoplastic effectors that suppress host immunity[10,11]. These intracellular and secreted factors enable the pathogen to more effectively exploit host tissues, particularly under conditions that promote rapid disease progression.

Plants rely on intracellular immune receptors, particularly NLRs, to detect pathogen invasion and trigger defense responses. Plants encode numerous NLR proteins that use diverse, well-characterized mechanisms to defend against pathogen invasion[12,13]. CC-NBS-LRR (CNL) receptors are central components of plant innate immunity, functioning as molecular switches that transition from an autoinhibited to an activated state upon pathogen detection[14]. In the resting state, the NBS domain binds ADP, the LRR domain maintains structural repression, and the CC domain remains sequestered to prevent unwarranted immune activation[14–16]. Pathogen effectors are sensed either directly by the LRR domain or indirectly through modifications of host guard proteins[14,17]. This recognition disrupts LRR-mediated inhibition and triggers ADP–ATP exchange in the NBS domain, enabling the receptor to adopt an open conformation[14,18]. The exposed CC domains then drive oligomerization of activated CNLs into a membrane-associated resistosome[14,19]. This resistosome acts as a calcium-permeable channel that initiates downstream defense signaling, including localized cell death to restrict pathogen spread[18,20,21].

Before activation, NLRs are tightly regulated to prevent unintended immune responses, with CC domains playing a central role in maintaining the receptor in an inactive state. Intramolecular interactions between the CC and NB-ARC or LRR domains act as autoinhibitory constraints, preventing spontaneous CC oligomerization and autoactivation[18,22]. Inactive NLRs are further stabilized by intermolecular interactions, existing in a dynamic equilibrium between monomeric receptors and multi-protein complexes. Notable examples include the ZAR1–ZED1 and ZAR1–ZRK complexes, which prevent premature activation while keeping the receptor ready for pathogen detection[23]. Together, these intramolecular and intermolecular mechanisms provide tight control over immune activation, enabling rapid defense responses while minimizing the risk of autoimmunity.

Heat shock proteins (HSPs), including HSP70 and HSP90, also play critical roles in modulating NLR protein function. HSPs can act as positive regulators by promoting NLR stability and complex assembly, or as negative regulators by preventing overactivation, in both plants and animals. Numerous studies have shown that HSP90s perform diverse functions in plant biology, including immunity, light signaling, chloroplast biology, and general growth and development[24,25]. Specifically, HSP90, together with the co-chaperones RAR1 and SGT1, modulates the activities of multiple plant NLR proteins, including MLA, RPM1, RPS2 and RPS4[26,27]. HSP90.2 and HSP90.3 lead to increased accumulation of immune receptors, including SNC1, RPS2 and RPS4[28]. Interestingly, SGT1 functions as a multifaceted co-chaperone, positively regulating NLR activation while also preventing excessive accumulation of receptors such as RPM1, RPS5, and SNC1[29,30]. This dual role likely reflects its engagement with multiple protein complexes during immune responses.

HSA32 is a heat-stress–inducible gene widely conserved across land plants but not classified among the classical HSP families. It encodes a 32-kD heat-stress-associated protein and occurs as a single-copy gene in Arabidopsis, rice, and tomato[31]. *HSA32* is a prominent downstream target of the master heat-stress transcription factors HsfA1a and HsfA1b in Arabidopsis[32] and of TaHsfA2–10 in wheat[33]. Functionally, HSA32 plays a key role in thermotolerance by stabilizing the chaperone HSP101, which in turn promotes HSA32 accumulation, forming a conserved positive feedback loop demonstrated in both Arabidopsis and rice[34,35]. In wheat, genes encoding multiple sHSPs (small heat shock proteins) are transcriptionally induced by elevated temperature[36,37], yet their tissue-specific contributions, particularly within the spike, a heat-sensitive organ critical for yield, is unknown. Many wheat sHSPs exhibit strong spatiotemporal specificity, as they are highly expressed during late developmental stages and in tissues frequently exposed to post-anthesis heat (spikes, filling grains, and mature leaves), suggesting that they might enable rapid responses to heat or pre–heat cues[36,37]. By contrast, several subfamilies (MI, CIX, and CV) show constitutive expression across all tissues and stages, display weaker heat inducibility, and experience lower selective pressure, implying that these groups may have undergone functional shifts from a canonical heat-shock responsiveness toward more general cellular roles[36].

Despite the central role of NLR receptors in safeguarding wheat against *F. graminearum*, how fungal effectors modulate NLR stability under high temperature conditions remains poorly understood. In particular, the regulatory mechanisms that balance NLR activation with environmental cues, such as heat-induced protein homeostasis, are largely unknown. Here, we identify a secreted effector from *F. graminearum*, FgUP7, that targets the wheat NLR TaRPM1. Furthermore, our work found an unexpected connection between NLR regulation and a heat-responsive chaperone protein, TaHSA32, and uncovered how effector interference with N-terminal CC-domain dynamics might shape immune outcomes. Together, these findings show how fungal pathogens attenuate NLR-mediated immunity and uncovered an underappreciated regulatory layer at the interface of temperature-modulated immune activation, protein stability, and pathogen virulence.

Results

FgUP7 contributes to the virulence of *F. graminearum* and suppresses plant basal immune responses

To identify pathogenicity-associated effectors of *F. graminearum*, we first analyzed 148 previously predicted candidates[11]. Transcriptome profiling across the mycelial stage and multiple infection time points (12, 24, 48, and 72 hpi)[38], identified 12 genes that were barely detectable in mycelia but strongly induced during host infection (Supplementary Fig. 1a, b). In parallel, a genome-wide survey in strain PH-1, together with expression analyses in Arabidopsis and in both susceptible (Sonalika) and resistant (Nobeoka) wheat genotypes[39], identified several pathogenicity-related candidates, including 11 genes associated with virulence. Among the overlapping candidates from both approaches, FGSG_03748 (hereafter designated FgUP7) stood out because of its infection-specific induction and effector-like characteristics, and because it was relatively conserved among *Fusarium* spp. (Supplementary Fig. 1c).

To determine whether FgUP7 was secreted, we used a yeast secretion assay and found that the predicted signal peptide of FgUP7 restored growth of an invertase-deficient yeast strain on YPRAA medium, similar to the positive control Avr1b (Fig. 1a, Supplementary Fig. 1d), showing that the N-terminal peptide of FgUP7 is functional in directing protein secretion. Transient expression in *Nicotiana benthamiana* further showed that FgUP7

localized to the nucleus and plasma membrane, and this localization pattern was not altered by deletion of the signal peptide (Supplementary Fig. 1e). Deletion of FgUP7 did not affect *F. graminearum* growth in vitro (Fig. 1b, c; Supplementary Fig. 2a, b) but markedly reduced virulence on wheat spikes (Fig. 1d, e), whereas complementation fully restored pathogenicity (Fig. 1d, e). To assess whether FgUP7 impacted plant basal immunity, we examined its effect on chitin-triggered responses in *N. benthamiana*. Transient expression of FgUP7 significantly suppressed the chitin-induced ROS burst compared with the GFP control (Fig. 1f). Consistently, co-expression of FgUP7 reduced BAX–induced cell death (Supplementary Fig. 2c) and led to decreased expression of the immunity-associated marker genes *NbPR1* and *NbPAD4* (Supplementary Fig. 2d). To further determine the role of FgUP7 in wheat basal defense, we quantified the expression of immune-related genes following pathogen inoculation. Compared to the wild-type strain, inoculation with the FgUP7 deletion mutant resulted in significantly higher transcriptional levels of *TaMAPK3*, *TaPR1*, and *TaFLS2* in wheat spikes (Supplementary Fig. 2e). Together, these results identify FgUP7 as a secreted effector essential for full virulence of *F. graminearum* on wheat and capable of suppressing multiple layers of plant immune responses.

FgUP7 targets the wheat NLR immune receptor TaRPM1 and accelerates its degradation

To identify host targets of FgUP7 in wheat, we performed a yeast two-hybrid screen and recovered the NLR immune receptor TaRPM1 as an interacting partner (Fig. 2a; Supplementary Table 1). TaRPM1 comprises canonical CC, NB-ARC and LRR modules (Supplementary Fig. 3a). We then performed yeast two-hybrid assays to individually test the CC, NB-ARC, and LRR domains of TaRPM1 for their ability to interact with FgUP7. Only the CC domain exhibited a robust interaction with FgUP7 (Fig. 2a). Consistently, luciferase complementation imaging (LCI) assays elicited strong luminescence signals when FgUP7-cLuc was co-expressed with TaRPM1-CC-nLuc or TaRPM1-NB-ARC-nLuc in *N. benthamiana* leaves, but not with full-length TaRPM1-nLuc, TaRPM1-LRR-nLuc, or the negative controls (Fig. 2b). These data support the notion that FgUP7 preferentially associates with the CC domain of TaRPM1.

To validate this interaction biochemically, we conducted in vitro pull-down assays using GST-tagged TaRPM1, TaRPM1-CC, TaRPM1-NB-ARC, and TaRPM1-LRR incubated with MBP-tagged FgUP7. Immunoblot analysis showed that FgUP7 could interact with TaRPM1, TaRPM1-CC and TaRPM1-NB-ARC (Fig. 2c), confirming the physical interaction between FgUP7 and the CC domain. Finally, microscale thermophoresis (MST) assays were used to further quantify these interactions. Both TaRPM1 and TaRPM1-CC displayed direct binding to FgUP7, with dissociation constants (*Kd*) of 70.61 μM and 5.44 μM, respectively, whereas no measurable binding was detected between FgUP7 and either the NB-ARC or LRR domains (Fig. 2d-g). Notably, the markedly lower *Kd* value for TaRPM1-CC indicates a substantially higher affinity, reinforcing that the CC domain is the primary interface for FgUP7 recognition.

Taken together, yeast two-hybrid, *N. benthamiana* LCI, in vitro pull-down, and MST assays all confirmed a strong interaction between FgUP7 and the TaRPM1-CC domain, whereas the interaction with full-length TaRPM1 appeared less robust. This discrepancy prompted us to investigate whether differences in protein stability across assay systems might account for this difference. Time-course incubation of recombinant proteins showed that full-length TaRPM1 is intrinsically unstable and undergoes gradual degradation, and that the presence of FgUP7 markedly accelerated this process (Supplementary Fig. 3b, c). By comparison, FgUP7 had negligible effects on the stability of the CC, NB-ARC or LRR domains (Supplementary Fig. 3d-f). Notably, FgUP7 itself also underwent degradation when incubated with full-length TaRPM1, suggesting that their association triggers mutual destabilization.

The CC domain of TaRPM1 self-interacts and triggers plant immune responses

The CC or TIR domains of NLRs are known to oligomerize and act as key determinants of immune activation[40–43]. Consistent with this, transient expression in *N. benthamiana* of either full-length TaRPM1 or its isolated CC domain both triggered cell death, indicating that the CC domain contributes to immune signaling (Fig. 3a). To assess whether TaRPM1 or TaRPM1-CC impacted plant basal immunity, we examined its effect on chitin-triggered responses in *N. benthamiana*. Transient expression of TaRPM1 or

TaRPM1-CC significantly enhanced the chitin-induced ROS burst compared with the HA control (Fig. 3b, c).

Because CNL proteins must remain strictly inactive in the absence of pathogen challenge, we hypothesized that TaRPM1 is likely autoinhibited through intramolecular interactions that shield the CC domain and prevent inappropriate oligomerization. Yeast two-hybrid assays showed that TaRPM1-CC interacted robustly with itself and with the NB-ARC domain, whereas no interaction was detected between the LRR and CC domains (Fig. 3d). We used LCI assays to further test whether TaRPM1 underwent self-association. When TaRPM1-CC-cLuc was co-expressed with TaRPM1-CC-nLuc or TaRPM1-NB-ARC-nLuc in *N. benthamiana* leaves, strong luminescence signals were detected, whereas no signals were observed upon co-expression with TaRPM1-LRR-nLuc or with the negative controls (Fig. 3e). These results demonstrate that the CC domain of TaRPM1 is capable of self-interaction.

To validate this interaction, we performed MST assays using MBP-tagged TaRPM1, TaRPM1-CC, TaRPM1-NB-ARC, and TaRPM1-LRR in combination with GST-tagged TaRPM1-CC. Consistent with the LCI results, TaRPM1-CC exhibited a strong self-association, with a dissociation constant (*Kd*) of 1.80 μM (Fig. 3f). Notably, in contrast to the canonical NLR model in which the LRR domain imposes autoinhibition through intramolecular CC–LRR contacts, we detected no measurable interaction between the CC and LRR domains. This finding suggests that TaRPM1 may adopt a regulatory configuration distinct from previously described NLRs.

TaRPM1 positively regulates wheat resistance to *F. graminearum*

Given the central role of TaRPM1 in immune signaling, we next examined its contribution to wheat resistance against *F. graminearum*. We identified EMS mutants of TaRPM1 in tetraploid wheat (Kronos), including alleles in the 2A and 2B subgenomes (*tarpm1-a* and *tarpm1-b*). Both mutants displayed enhanced susceptibility (Fig. 3g), accompanied by a significant increase in disease index (Fig. 3h). We also identified a hexaploid mutant in KN9204 (*tarpm1*-8804), which similarly had markedly expanded lesions on coleoptiles compared with the wild type (Supplementary Fig. 4).

Given the importance of CC-domain–mediated activation, we generated CRISPR/Cas9-edited lines targeting the CC domain and obtained two independent knockout types (Supplementary Fig. 5a). *TaRPM1*-KO plants developed more severe Fusarium head blight symptoms than wild-type plants after inoculation, showing significantly elevated disease indices (Fig. 3i, j). In contrast, transgenic wheat overexpressing *TaRPM1* exhibited enhanced resistance, with fewer symptoms and lower disease severity scores (Fig. 3i, j; Supplementary Fig. 5b).

To evaluate the potential breeding applicability of TaRPM1, we assessed key agronomic traits of *TaRPM1*-overexpressing and CRISPR/Cas9-edited lines under greenhouse conditions. No significant differences were detected in plant height, thousand-grain weight, grain width, and grain length compared to those measures in control plants (Supplementary Fig. 6). These results indicate that enhanced *TaRPM1* expression does not affect major growth or yield-related traits while conferring increased resistance to *F. graminearum*.

FgUP7 targets the N-terminal region of the TaRPM1 CC domain to disrupt CC self-interaction

To investigate the effect of FgUP7 on TaRPM1, we first assessed whether FgUP7 influenced the self-association of the TaRPM1 CC domain. In yeast three-hybrid assays, co-expression of AD-TaRPM1-CC and TaRPM1-CC-FgUP7 significantly impaired growth on SD–Leu-Trp-His-Met medium, indicating a reduced CC–CC interaction in the presence of FgUP7 (Fig. 4a). Consistently, LCI assays in *N. benthamiana* showed a marked decrease in luminescence between TaRPM1-CC-nLuc and TaRPM1-CC-cLuc upon co-expression with FgUP7, than in the FgUP7-free control (Fig. 4b). MST further confirmed these observations: TaRPM1-CC exhibited strong self-association with a dissociation constant (*Kd*) of 1.61 μM, whereas the addition of FgUP7 disrupted this self-interaction (Fig. 4c). To further examine the effect of FgUP7 on TaRPM1-CC self-association, we performed competitive pull-down assays. Equimolar GST-TaRPM1-CC and MBP-TaRPM1-CC were incubated with MBP beads in the presence of increasing concentrations of HIS-FgUP7. The amount of GST-TaRPM1-CC co-precipitated with

MBP-TaRPM1-CC decreased in a dose-dependent manner, demonstrating that FgUP7 competitively disrupts TaRPM1-CC self-interaction (Fig. 4d).

Unlike classical pathogen effectors, which often target the leucine-rich repeat (LRR) domain of NLRs to trigger their activation and oligomerization, yeast three-hybrid, competitive LCI, MST, and competitive pull-down assays showed that FgUP7 strongly inhibits the self-interaction of the TaRPM1-CC domain (Fig. 4a-d), directly interfering with the oligomerization required for resistosome formation. To further define the key region of TaRPM1-CC recognized by FgUP7, we generated three N-terminal truncations of the CC domain (Fig. 4e). Yeast two-hybrid assays showed that FgUP7 specifically interacted with the N-terminal 1–35 aa region of TaRPM1-CC (Fig. 4f), indicating that FgUP7 is recognized through the N-terminal portion of the CC domain and competitively inhibits the self-association of this region.

TaHSA32 interacts with TaRPM1 and stabilizes TaRPM1

Previous experiments failed to detect a direct interaction between the CC and LRR domains of TaRPM1, implying that additional, as-yet-unidentified accessory proteins might act to shield or sequester the CC domain and maintain the protein in an inactive state. To identify potential TaRPM1-interacting proteins, we performed a yeast two-hybrid screen and found that the heat shock–associated protein TaHSA32 interacts with TaRPM1 (Fig. 5a, Supplementary Table 2, Supplementary Fig. 7a). Co-localization assays and BiFC assays in *N. benthamiana* confirmed that TaHSA32 and TaRPM1 co-localize in planta (Supplementary Fig. 7b, c). To determine the interacting domains, we performed yeast two-hybrid assays and found that TaHSA32 interacts with the CC and NB-ARC domains of TaRPM1 (Fig. 5a; Supplementary Fig. 7a). Consistently, LCI assays measured strong luminescence signals when TaHSA32-cLuc was co-expressed with TaRPM1-nLuc, TaRPM1-CC-nLuc, or TaRPM1-NB-ARC-nLuc, but not with TaRPM1-LRR-nLuc or in the controls (Fig. 5b). MST further confirmed a direct, high-affinity interaction between TaHSA32 and TaRPM1-CC (Kd = 1.32 μM), whereas no measurable binding was detected with full-length TaRPM1, TaRPM1-NB-ARC, or TaRPM1-LRR (Fig. 5c-f). Together, these results demonstrate that TaHSA32 primarily targets the TaRPM1 CC domain, with weaker or no interactions with other domains.

To determine whether TaHSA32 recognizes the same region of TaRPM1-CC as FgUP7, we performed yeast two-hybrid assays using TaRPM1-CC truncations. TaHSA32 showed a strong interaction with the N-terminal 1–35 aa of TaRPM1-CC and a weaker interaction with the 24–66 aa region (Supplementary Fig. 8). These data indicate that the N terminus of the CC domain serves as the primary recognition region for both TaHSA32 and FgUP7, while TaHSA32 additionally exhibits weak binding to the central portion of the CC domain.

TaHSA32 is strongly induced under heat stress and functions as a molecular chaperone, recognizing misfolded proteins and preventing their aggregation to maintain protein stability[44,45]. To investigate whether TaHSA32 influences the stability of TaRPM1, we first assessed the self-association of TaRPM1-CC using MST. TaRPM1-CC displayed strong self-interaction, with a dissociation constant (*Kd*) of 2.54 μM; however, the addition of TaHSA32 markedly disrupted this self-association (Fig. 5g). We next used a yeast three-hybrid assay to determine whether TaHSA32 affects the strength of CC-domain self-interaction. Co-expression of AD-TaRPM1-CC and TaRPM1-CC-TaHSA32 significantly impaired growth on SD–Leu-Trp-His-Met medium, indicating reduced CC–CC interaction in the presence of TaHSA32 (Fig. 5h). Consistently, LCI assays in *N. benthamiana* showed a marked decrease in luminescence between TaRPM1-CC-nLuc and TaRPM1-CC-cLuc when TaHSA32 was co-expressed, compared with the TaHSA32-free control (Fig.5i). Together these results demonstrate that TaHSA32 suppresses self-interaction of the TaRPM1 CC domain (Fig. 5g-i).

In addition, in vitro co-incubation of purified proteins demonstrated that TaHSA32 stabilizes both full-length TaRPM1 and the CC domain at 37 °C (Fig. 5j, k). Collectively, these results indicate that TaHSA32 is a key factor in maintaining TaRPM1 in an inactive state, with the NB-ARC domain and TaHSA32 together stabilizing the protein.

TaHSA32 negatively regulates wheat resistance to *F. graminearum* without affecting major agronomic traits

To investigate whether TaHSA32 affects disease resistance, we first analyzed its transcript levels during *F. graminearum* infection of wheat heads. Expression of *TaHSA32* rapidly increased after infection (Fig. 6a). We generated *TaHSA32*-

overexpressing (OE) transgenic lines in the wheat cultivar Fielder (Fig. 6b), with expression levels increased 50–80-fold in lines OE-5 OE-23 and OE-32. Infection assays showed that these three TaHSA32-OE plants were less resistant to *F. graminearum*, than wild-type Fielder (Fig. 6d, e). Conversely, we generated *TaHSA32* knockout (KO) lines using CRISPR/Cas9 (Fig. 6c). Two independent KO types were selected for further analysis. Upon inoculation with the wild-type strain, *TaHSA32*-KO plants displayed milder symptoms and significantly lower disease indices than Fielder plants (Fig. 6d, e). These results indicate that TaHSA32 functions as a negative regulator of wheat resistance to *F. graminearum*. We also assessed key agronomic traits to examine potential effects of TaHSA32 on growth. No significant differences were observed between *TaHSA32*-OE, KO, and control plants in thousand-grain weight, grain width, and grain length (Fig. 6f-i), indicating that TaHSA32 modulates disease resistance without affecting major growth traits.

FgUP7 competitively binds TaHSA32, destabilizing the TaRPM1–HSA32 molecular lock and inhibiting NLR activation

Under high-temperature conditions, TaHSA32 is strongly induced (Supplementary Fig. 9), and its elevated accumulation allows it to interact with and stabilize TaRPM1 while simultaneously dampening wheat resistance to *F. graminearum*. This dual effect raises an important question as to how TaHSA32 and pathogen-derived effectors collectively modulate TaRPM1 activity during infection.

To dissect the relationship among FgUP7, TaHSA32 and TaRPM1, we first examined whether TaHSA32 associates with the secreted effector FgUP7. Yeast two-hybrid assays showed interaction between TaHSA32 and FgUP7 (Fig. 7a). Consistently, LCI showed strong luminescence when FgUP7 and TaHSA32 were co-expressed in *N. benthamiana*, whereas no signal was detected in the controls, further confirming their association (Fig. 7b). Subcellular co-localization analysis also supported the interaction between FgUP7 and TaHSA32 (Supplementary Fig. 10a).

To determine whether FgUP7 affects the TaRPM1-TaHSA32 interaction, we next quantified their binding affinity using MST. TaRPM1-CC bound to TaHSA32 with high affinity (Kd = 1.31 μM), whereas the addition of FgUP7 disrupted this interaction (Fig.

7c). In line with this result, yeast three-hybrid assays showed that co-expression of AD–TaRPM1-CC with TaHSA32-FgUP7 markedly reduced growth on SD–Leu-Trp-His-Met medium. Similarly, co-expression of AD-TaHSA32 with TaRPM1-CC-TaHSA32 also impaired growth (Fig. 7d; Supplementary Fig. 10b), indicating that FgUP7 interferes with the TaRPM1-CC-TaHSA32 association. LCI assays in *N. benthamiana* showed a marked decrease in luminescence between TaRPM1-CC-nLuc and TaHSA32-cLuc when FgUP7 was co-expressed, compared with the FgUP7-free control (Fig.7e). Finaly, in vitro pull-down assays using recombinant HIS-FgUP7, GST-TaRPM1-CC and MBP-TaHSA32 further validated this inhibitory effect. When equal amounts of GST-TaRPM1-CC and MBP-TaHSA32 were incubated with MBP beads, increasing concentrations of FgUP7 progressively reduced the amount of GST-TaRPM1-CC retained with MBP-TaHSA32, in a dose-dependent manner (Fig. 7f).

These results indicate that FgUP7 preferentially binds TaHSA32, competitively displacing it from the TaRPM1 complex. This dual action destabilizes the molecular lock formed by TaHSA32 and the NB-ARC domain, while simultaneously preventing CC-domain oligomerization, thereby suppressing TaRPM1 activation and dampening NLR-mediated immune signaling during pathogen attack.

Conserved function of RPM1 in *Brachypodium distachyon*

To further evaluate the conservation of this regulatory axis in monocots, we examined the function of the TaRPM1 ortholog in the model grass *B. distachyon* (Supplementary Fig. 11a). BdRPM1 also possesses the typical CC, NB-ARC, and LRR domains (Supplementary Fig. 11b). To investigate whether expression of *BdRPM1* affects disease resistance, we first analyzed its transcript levels during infection of *B. distachyon* spikelets with *F. graminearum*, and found that expression was rapidly increased post-infection (Supplementary Fig. 11c). A CRISPR-mediated knockout of *BdRPM1* showed markedly enhanced susceptibility to *F. graminearum* (Supplementary Fig. 11d-f), demonstrating that RPM1-mediated defense is functionally conserved in this model grass species. Biochemical assays further showed that BdRPM1 physically interacts with BdHSA32 (Supplementary Fig. 12), mirroring the interaction pattern observed in wheat, supporting evolutionary conservation of the RPM1–HSA32 module within the examined

monocot species. This cross-species conservation underscores the broader relevance of the HSA32–RPM1 axis and suggests that stabilizing HSA32–NLR complexes, or disrupting effector interference at this node, could offer a promising strategy for resistance breeding in cereals.

Discussion

Plant NLR receptors are classically thought to perceive pathogen-derived molecules through their LRR domains, and most characterized effectors interfere with LRR-mediated recognition[14,46]. The coiled-coil (CC) domain, however, serves as the nucleation module for resistosome assembly, undergoing stimulus-dependent oligomerization that triggers downstream defense responses[46,47].

Our findings indicate a synergistic interplay between heat stress and pathogen attack in suppressing NLR-mediated immunity. The heat-inducible protein TaHSA32 highlights temperature as a critical environmental factor that sets the activation threshold for NLRs. Under conditions of combined heat and pathogen presence, the effector FgUP7 exhibits enhanced activity, suggesting that elevated temperatures may potentiate effector-mediated suppression of immune signaling.

We demonstrate that FgUP7 acts as a secreted virulence factor that suppresses wheat immunity by directly targeting the NLR protein TaRPM1. Unlike canonical effectors that interfere with NLR activation by binding to the LRR domain[47,48], FgUP7 shows strong affinity for the TaRPM1 coiled-coil (CC) domain, particularly the N-terminal helical segment (Fig. 2a, Fig. 4f). This interaction with FgUP7 disrupts CC-domain self-association, thereby blocking the early oligomerization step required for NLR activation. Intriguingly, our data also showed that FgUP7 accelerates the degradation of full-length TaRPM1 (Supplementary Fig. 3c), suggesting that effector-mediated destabilization of immune receptors contributes to pathogenic success. However, the precise degradation mechanism remains unclear. Plant NLR homeostasis is tightly governed by post-translational protein turnover. The ubiquitin-26S proteasome system is known to control the steady-state levels of several NLRs; for example, the F-box E3 ligase CPR1 targets the autoimmune NLR SNC1 for ubiquitination and proteasomal degradation[49]. Moreover, the actions of pathogen effectors such as the *Phytophthora infestans* protein Pi06432 and

the *Magnaporthe oryzae* effector AvrPiz-t illustrate how microbes hijack the host proteasome machinery to attenuate immune signaling[49–52]. In addition to proteasomal degradation, selective autophagy has emerged as a complementary quality control pathway in plant immunity. Autophagy receptors, including NBR1 and related adaptors, mediate the clearance of ubiquitinated protein aggregates and immune regulators, and accumulating evidence indicates that autophagy shapes immune receptor abundance and downstream signaling[53]. Intriguingly, FgUP7 itself also becomes destabilized upon binding TaRPM1 (Supplementary Fig. 3c), raising the possibility of a reciprocal degradation mechanism. Our findings suggest that FgUP7 suppresses basal immunity by targeting the CC domain of TaRPM1, compromising both receptor stability and activation.

As NLR activated downstream signaling often results in cell death and a high fitness cost for the plant, NLRs need to be tightly modulated in the absence of pathogens. NLRs are maintained in an inactive state by coordinated intramolecular and intermolecular interactions. Our results showed that the NLR protein RPM1 associates with TaHSA32, a heat-responsive chaperone-like protein that functions as a stabilizing cofactor binding both the CC and NB-ARC domains of TaRPM1. At 20 °C, TaHSA32 is weakly expressed and the system exists in a dynamic equilibrium between TaRPM1 alone and the TaRPM1–HSA32 complex (Fig. 7f). As temperature increases, NLR proteins become intrinsically unstable and rely on host chaperones such as HSP90, SGT1 and RAR1 to maintain proper folding and activation competence[54,55]. Small heat shock proteins (sHSPs) also act as ATP-independent molecular chaperones that bind misfolded or heat-labile proteins to prevent aggregation and maintain functional stability[45]. Yet, their involvement in modulating NLR conformational states has remained largely unexplored. Here, we show that the small heat shock protein TaHSA32 binds TaRPM1 and inhibits CC-domain oligomerization, maintaining the receptor in an auto-inhibited monomeric state under elevated temperatures. This mechanism maintains RPM1 folding and prevents its unintended activation under heat stress. Our data showed that under elevated temperatures, the *F. graminearum* effector FgUP7 disrupts the TaRPM1–TaHSA32 complex by preferentially binding TaHSA32. This displacement compromises the protective protein-folding environment maintained by sHSPs, resembling previously

reported cases in other NLR systems where pathogen effectors target the HSP90–SGT1–RAR1 chaperone complex[54,56], suggesting that FgUP7 represents a functionally analogous mode of chaperone hijacking.

These findings support a model in which FgUP7 suppresses NLR immunity via a dual strategy: it binds the CC domain to block early NLR oligomerization and accelerates degradation of full-length TaRPM1, reducing cellular surveillance against *F. graminearum*. In contrast, heat-induced TaHSA32 stabilizes TaRPM1, maintaining immune competence under fluctuating temperatures. By competing with TaHSA32 for binding, FgUP7 removes this protective layer, leaving TaRPM1 vulnerable to destabilization. This antagonistic interplay explains how elevated temperatures and pathogen effectors synergistically undermine NLR-mediated immunity (Fig. 7f).

The conservation of this module in another monocot also raises broader evolutionary and translational implications. NLR activation in cereals has long been considered less understood than in dicots, partly due to the complexity and redundancy of grass immune receptors[57]. The finding that RPM1 and its HSA32 cofactor operate via a conserved mechanism, suggesting that monocot NLRs generally depend on heat- and stress-responsive chaperone-like proteins for activation competence (Supplementary Fig. 12), consistent with studies showing NLR stability and activation rely on accessory proteins such as HSP90 co-chaperones and other thermal regulators[54]. Our results position HSA32-like proteins as previously underappreciated components that buffer NLRs against environmental fluctuations, especially temperature shifts known to suppress immunity[45].

Together, these findings identify the HSA32–RPM1 regulatory node as a promising entry point for engineering *Fusarium*-resistant cereals. Enhancing the stability of this node may facilitate the development of cultivars with durable, climate-resilient immunity.

Methods

Growth conditions of plant materials and fungal strains

The wheat cultivar Fielder, Kronos and KN9204 were cultured in a greenhouse at 22 °C with a light/dark cycle of 16/8 h, for pathogen inoculation assays. KN9204 (winter

wheat) were germinated and subsequently transferred to soil, where they were grown at 4°C in the dark for 45 days. The heading date of each wheat plant was determined as the number of days from sowing to the stage when 50% of the spikes had fully emerged.

The EMS mutants from the tetraploid variety “Kronos” were produced by Dr. Jorge Dubcovsky's group at the University of California, Davis[58], and were backcrossed two times before analysis. The EMS mutants from the tetraploid variety “KN9204” were produced by Dr. Jun Xiao's group at the Institute of Genetics and Developmental Biology, Chinese Academy of Sciences[59], and were backcrossed two times before analysis.

Fielder of transgenic wheat T_2 generation lines were grown in the experimental field of the Peking University Institute of Advanced Agricultural Sciences, Shandong, China (119°18’E, 36°16’N). For the field experiment, each line was planted in three replicates. Each replicate consisted of 10 rows, each 1.5 meters long, with a row-to-row spacing of 0.20 meters.

For agronomic trait measurements, grains were harvested from the spike, and 150 grains were randomly selected for analysis. A normal distribution analysis of the selected grains confirmed that grain sizes followed a normal distribution, ensuring the representation of grains from both the apical and basal regions. Grain width, grain length, and thousand-grain weight were measured using a Wanshen SC-G seed detector (Hangzhou Wanshen Detection Technology Co., Ltd.). Grain length and width were measured for more than 70 grains. Agronomic traits, including grain length, grain width, thousand-grain weight, were measured with 15 representative plants.

N. benthamiana was grown in a growth chamber at 21–23 °C under a 14-h light and 10-h dark photoperiod. The *F. graminearum* PH-1 wild-type and mutant isolates were grown in the dark at 25 °C on potato dextrose agar (PDA) medium.

F. graminearum **transformation**

The protoplasts were generated through the incubation of young *F. graminearum* hyphae produced by conidia in yeast extract peptone dextrose (YEPD) medium with an enzymatic lysis buffer (25 g/L driselase and 5 g/L lysing enzyme in 1.2 M KCl) for 2–3 h at 28°C. The lytic product was filtered through Miracloth, and protoplasts were harvested

in STC buffer (200 g/L sucrose, 0.5 M Tris-Cl, pH 8.0, 0.05 M $CaCl_2$) at a concentration of 10^5 cells/mL. We employed a split-marker disruption system to generate *ΔFgUP7* mutants[60]. The strategy for deleting *FgUP7* is illustrated in Supplementary Fig. 2A. First, the 5' and 3' flanking sequences of *FgUP7* were amplified from genomic DNA by polymerase chain reaction (PCR) with FgUP7LF/FgUP7LR and FgUP7RF/FgUP7RR primers, respectively. The resulting amplicons were then fused with the 5' and 3' fragments of the hygromycin phosphotransferase cassette (hph) using double-jointed PCR.

Next, we amplified the overlapping fragments with FgUP7LFNest/HYRNest and NYGFNest/FgUP7RRNest primers. The fusion PCR product was transformed into *F. graminearum* protoplasts using a PEG-mediated transformation method[61]. The 1.9-kb region containing *FgUP7* and its promoter was ligated into the pKNTG vector and transformed into *ΔFgUP7*-7 mutant protoplasts for the complementation assay. The primers used in this study are listed in Supplementary Data 3.

Generation of transgenic wheat and *B. distachyon* plants

For CRISPR/Cas9 editing of *TaRPM1* and *TaHSA32*, the binary vector CasV2-GRF4-GIF1-TaU3-gRPM1 or CasV2-GRF4-GIF1-*TaU3*-gHSA32 was transformed into the wheat variety Fielder via *A. tumefaciens* strain EHA105. Regenerated seedlings with Basta resistance were selected for further analysis. Gene fragments containing the target sites were amplified by PCR with gene-specific primers, and gene editing was confirmed by Sanger sequencing. T3 plants with homozygous mutations were used for further analysis. To overexpress *TaRPM1* and *TaHSA32*, the binary vector p1300-*UBQ10*-preTaRPM1 or p1300-*UBQ10*-preTaHSA32 was transformed into the wheat variety Fielder. TaRPM1 and TaHSA32 overexpression in transgenic lines was confirmed by RT–qPCR with the gene-specific primers listed in Supplemental Table 3.

For CRISPR/Cas9 editing of *BdRPM1*, the binary vector pYLCRISPR-*OsU3*-gRPM1 was transformed into the *B. distachyon* variety Bd21-3 via *A. tumefaciens* strain EHA105. Regenerated seedlings with Basta resistance were selected for further analysis. Gene fragments containing the target sites were amplified by PCR with gene-specific primers, and gene editing was confirmed by Sanger sequencing.

Infection assays

Conidia were collected from the carboxymethyl cellulose (CMC) medium and reached 10^6 spores/mL in sterile distilled water. A 10 μL conidium suspension was injected into the fourth or fifth spikelet from the base of flowering wheat heads of cultivars Fielder or Kronos. The inoculated wheat heads were incubated in bags at high humidity for 48 h. The number of infected spikelets in each wheat head was recorded as the disease index 14 days after inoculation.

ROS accumulation detection

Plugs (6 mm diameter) were punched from *N. benthamiana* leaves expressing FgUP7 and incubated in water in a 96-well plate to examine the ROS burst. After 18 h, 200 μL of luminescence detection buffer (1 μM chitin, 100 mM luminol, and 20 mg/mL horseradish peroxidase) was added to plates, and the luminescence was recorded by a microplate reader for 60 min. The data from twelve biologically independent samples were recorded.

RNA extraction and RT–qPCR assays

Total wheat flowering head RNA was extracted using the SPARKeasy New Plant RNA Extraction Kit (SparkJade, Jinan, China) following the manufacturer's instructions. First-strand complementary DNA (cDNA) was synthesized using a SPARKscript II All-in-one RT SuperMix for qPCR (With gDNA Eraser) (SparkJade, Jinan, China) according to the manufacturer's protocol. RT–qPCR was conducted on a QuantStudio™ 5 Real-Time PCR System (Applied Biosystems, Thermo Fisher Scientific) using 2×SYBR Green qPCR Mix (with ROX), following the manufacturer's protocol, to quantify the expression of target genes and verify transgenic overexpression or silencing in wheat. *FgActin* or *TaActin* was used as an endogenous reference gene, and the data were analyzed using the comparative $2^{-\Delta\Delta Ct}$ method. Each experiment included three independent biological replicates.

Yeast two-hybrid and tri-hybrid assays

Total RNA was extracted from the wheat flowering heads of Fielder inoculated with PH-1 at 0 and 72 hpi to construct the yeast two hybrid library. The FgUP7$^{\Delta SP}$ coding

sequence was cloned into the pGBKT7 vector for library screening. The constructed pGBKT7-FgUP7$^{\Delta SP}$ was co-transformed with library plasmids into the Y2HGold yeast strain. Yeast colonies grown on SD–Trp-Leu-His-Ade were isolated as the putative targets.

The CDSs of targets were cloned into pGADT7 and then transformed in pairs into the yeast strain Y2HGold for point-to-point verification of interactions between FgUP7$^{\Delta SP}$ and candidate targets. The relevant plasmid combinations were introduced into yeast cells, and transformants were selected on synthetic drop-out (SD) medium devoid of Trp and Leu. Transformants were transferred to a medium devoid of Trp, Leu, His, and Ade to investigate growth. The FgUP7$^{\Delta SP}$, and TaRPM1, and TaRPM1-CC, and TaHSA32, were ligated into the pBridge vector to perform the yeast three-hybrid assays. The pGADT7-TaRPM1-CC and pBridge-TaHSA32-FgUP7$^{\Delta SP}$, or pGADT7-TaRPM1-CC and pBridge-FgUP7$^{\Delta SP}$-TaHSA32, or pGADT7-TaRPM1-CC and pBridge-TaRPM1-CC-TaHSA32, or pGADT7-TaRPM1-CC and pBridge-TaRPM1-CC-FgUP7$^{\Delta SP}$ constructs were transformed into the Y2HGold yeast strain. The transformants were grown on SD–His-Leu-Trp or SD–His-Leu-Trp-Met plates.

Assays for the function of the SP of FgUP7

The predicted SP (17 aa) of FgUP7 was cloned into the pSUC2 vector[62] that carries the yeast SUC2 gene deleted of its SP sequence. The resulting SP–SUC2 construct was transformed into the yeast suc2 mutant YTK12[63] and assayed for growth on CMD-W (0.67% yeast nitrogen base without AAs, 0.075% tryptophan dropout supplement, 2% sucrose, 0.1% glucose, and 2% agar) and YPRAA medium plate (1% yeast extract, 2% peptone, 2% raffinose, and 2 μg/ml antimicyn A)[64]. Transformants of YTK12 carrying the empty pSUC vector or pSUC2-Avr1b^{SP}[65] were used as the negative and positive controls, respectively. The invertase enzymatic activity was detected by the reduction of 2,3,5-triphenyltetrazolium chloride (TTC) to insoluble red colored 1,3,5-triphenylformazan (TPF).

Luciferase complementation imaging assay

The coding sequences of FgUP7$^{\Delta SP}$, TaRPM1 (and its truncations TaRPM1-CC, -NB-ARC, and -LRR), and TaHSA32, were cloned into the pCambia1300-cLuc vector, constructed C-terminal luciferase fusions. Similarly, these sequences were cloned into the pCambia1300-nLuc vector, constructed N-terminal luciferase fusions. These constructs were transformed into the *A. tumefaciens* strain GV3101 and co-agroinfiltrated into *N. benthamiana* leaves using an induction buffer (10 mM MES, pH 5.8, 10 mM $MgCl_2$, and 100 mM acetosyringone). After 72 h, 1 mM D-luciferin was smeared on the infiltrated *N. benthamiana* leaves, and the luminescence signals were photographed using a NightSHADE evo LB 985N Chemiluminescent Imaging System.

BiFC and co-localization assays

The coding region of TaHSA32 was fused into the pCambia1300-YFPC vector, and the TaRPM1 coding sequence was cloned into the pCambia1300-YFPN vector. The fusion vectors TaHSA32-YFPC and TaRPM1-YFPN were transformed into *A. tumefaciens* strain GV3101 and transiently co-expressed in *N. benthamiana* leaves. After 48 h, the GFP fluorescence signals in the infiltrated leaves were observed using a confocal microscope.

To determine the co-localization between FgUP7$^{\Delta SP}$/TaRPM1 and TaHSA32, the coding sequence of FgUP7$^{\Delta SP}$ or TaRPM1 was fused into the pCambia1300-GFP vector, and the TaHSA32 coding sequence was cloned into the pCambia1300-mRFP vector. *A. tumefaciens* strains GV3101 containing the fused constructs were co-infiltrated into *N. benthamiana* leaves. The GFP and mRFP signals were detected by confocal microscopy.

In vitro pulldown assay

The pGEX-4T, pMAL-c2X, and pET32a vectors were used to express the GST-, MBP-, and HIS-tagged proteins, respectively. Recombinant pGEX-4T-TaRPM1 (and its truncations TaRPM1-CC, -NB-ARC, and -LRR), pMAL-FgUP7$^{\Delta SP}$, pMAL-TaHSA32, pMAL-TaRPM1-CC, and pET32a-FgUP7$^{\Delta SP}$ were introduced into *E. coli* BL21 (DE3). Cultures were induced with 0.5 mM isopropylthio galactosidases (IPTG) at 16 °C for 16 h with shaking at 200 rpm.

For verifying the interactions of TaRPM1 (and its truncations TaRPM1-CC, -NB-ARC, and -LRR)–FgUP7$^{\Delta SP}$, MBP beads were first added to the *E. coli* crude extract containing the MBP-FgUP7$^{\Delta SP}$ recombinant protein at 4 °C for 2 h. After removing the supernatant, the beads were washed three times with MBP binding buffer and mixed with GST-TaRPM1 (and its truncations TaRPM1-CC, -NB-ARC, and -LRR) crude extract at 4 °C for 2 h. Then the beads were enriched, washed with MBP binding buffer, and heated at 100 °C in SDS loading buffer for 5 min for the western blot analysis using anti–GST, or anti–MBP antibodies.

To detect the role of FgUP7$^{\Delta SP}$ in the interaction between TaRPM1-CC and TaHSA32, recombinant MBP-TaHSA32, GST-TaRPM1-CC, and HIS-FgUP7$^{\Delta SP}$ proteins were first purified. Then, equal amounts of GST-TaRPM1-CC and MBP-TaHSA32 fusion proteins were co-incubated with different amounts of HIS-FgUP7$^{\Delta SP}$ protein (0×, 5×, 10×, and 20×) before mixing with MBP beads.

MST analysis

Binding of recombinant MBP-FgUP7$^{\Delta SP}$, MBP-TaHSA32 or MBP-TaRPM1-CC and MBP control proteins with TaRPM1, TaRPM1-CC, TaRPM1-NB-ARC, TaRPM1-LRR was measured by MST in a Monolith NT.115 instrument (NanoTemper, Germany). The samples were loaded into the Monolith NT.115 standard capillaries and measured with 20% LED power and 40% MST power. The *KD*-fit function of the Nano Temper Analysis Software (V.2.3) was used to fit the curve and calculate the value of the dis-sociation constant (*Kd*).

Protein degradation assays

The in vitro protein degradation assays were performed as described previously[66]. In brief, 1 μg purified GST-TaRPM1 (and its truncations TaRPM1-CC, -NB-ARC, and -LRR) was co-incubated with a total of 1 μg MBP-FgUP7$^{\Delta SP}$ or MBP-TaHSA32 for 0, 2, 4, and 6 h before mixing. The GST-TaRPM1 (and its truncations TaRPM1-CC, -NB-ARC, and -LRR) was subjected to immunoblot analyses with anti–GST antibody. Meanwhile, western blot analysis using anti–MBP antibodies.

Bioinformatic analysis

The signal peptide of effector candidates was predicted by SignalP 6.0[67] and TargetP 2.0[68]. Identification of FgUP7 homologs was performed against the NCBI database based on BLASTp searches. Unrooted phylogenetic trees were constructed using MEGA 7 with the neighbor-joining method[69].

Statistics and reproducibility

E-BLOT Touch Imager XLi was used for WB data collection. All confocal micrographs were collected by Nikon A1HD25-SIM S. All representative experiments, such as micrographs and co-immunoprecipitations, were performed at least twice with similar results. GraphPad Prism 10.1.2 and Microsoft Office Excel were used for statistical analysis. Statistics were performed using one-way analysis of variance (ANOVA) tests or unpaired one-tailed Student's *t*-test. Data are reported as the mean ± SD. All analyses were performed on a minimum of three biological replicates unless otherwise specified. No data were excluded from the analyses. The investigators were not blinded to allocation during experiments and outcome assessment.

Data availability

Sequence data generated in this study are found in the EMBL library (http://plants.ensembl.org/index.html) under the following accession numbers: TaRPM1, TraesCS2B02G435600; TaHSA32, TraesCS7A02G451100; BdRPM1, BRADI_5g17527; BdHSA32, BRADI_1g32990.

Acknowledgements

This work was supported by Taishan Scholar Foundation of Shandong Province (tsqn202103162, tsqn202211093), Key R&D Program of Shandong Province, China (2024CXPT072), the Natural Science Foundation of Shandong Province (SYS202206), National Natural Science Foundation of China (32172387). We are grateful to Dr. Jun Xiao at the Institute of Genetics and Developmental Biology, Chinese Academy of Sciences, for providing the EMS-induced mutants of the hexaploid genotype KN9204. We thank Dr. Shikui Song of Peking University Institute of Advanced Agricultural Sciences for his technical guidance on the genetic transformation techniques in wheat and *B. distachyon*. We thank Dr. Sheila McCormick (UC Berkeley and USDA Plant Gene

Expression Center) and Dr. Weiguo Zhang (Northwest University) for valuable suggestions.

Author Contributions

Y.C and Q.W designed and supervised the study and wrote the manuscript. Y.W performed the experiments, analyzed the data and wrote the manuscript. X.L, C.X, F.Z, L.Z, Q.Z, and Y.S performed the experiments and analyzed the data. Z.W conducted all microscale thermophoresis experiments and performed the corresponding data analysis. L.Y performed all transformations and characterization of *F. graminearum* in this study. Z.Q performed data analysis and participated in manuscript revision. J.W provided EMS mutants from the tetraploid variety “Kronos” and participated in manuscript revision. Y.L and J.Q performed the genetic transformation of wheat and *B. distachyon*. Y.C and Q.W revised the manuscript and provided the funding for this research. All authors contributed to the article and approved the submitted version.

Declaration of interests

The authors declare no competing interests.

References

1. Chen, Y., Kistler, H. C. & Ma, Z. *Fusarium graminearum* Trichothecene Mycotoxins: Biosynthesis, Regulation, and Management. *Annu. Rev. Phytopathol.* **57**, 15–39 (2019).
2. Jung, J.-Y. *et al.* Adapting to the projected epidemics of Fusarium head blight of wheat in Korea under climate change scenarios. *Front. Plant Sci.* **13**, (2022).
3. Parry, D. W., Jenkinson, P. & McLEOD, L. Fusarium ear blight (scab) in small grain cereals—a review. *Plant Pathology* **44**, 207–238 (1995).
4. Brown, N. A., Urban, M., van de Meene, A. M. L. & Hammond-Kosack, K. E. The infection biology of *Fusarium graminearum*: Defining the pathways of spikelet to spikelet colonisation in wheat ears. *Fungal Biology* **114**, 555–571 (2010).
5. Garcia, M.-A. *et al.* Ecophysiological behavior of major Fusarium species in response to combinations of temperature and water activity constraints. *Applied and Environmental Microbiology* **91**, e01832–24 (2025).

6. Manstretta, V., Morcia, C., Terzi, V. & Rossi, V. Germination of Fusarium graminearum Ascospores and Wheat Infection are Affected by Dry Periods and by Temperature and Humidity During Dry Periods. *Phytopathology*® **106**, 262–269 (2016).
7. Ingram, B. *et al. Fusarium graminearum* and zearalenone in wheat: A water activity–temperature model. *Fungal Biology* **129**, 101572 (2025).
8. Jia, L.-J. *et al.* A linear nonribosomal octapeptide from *Fusarium graminearum* facilitates cell-to-cell invasion of wheat. *Nat Commun* **10**, 922 (2019).
9. Yun, Y. *et al.* Functional analysis of the *Fusarium graminearum* phosphatome. *New Phytologist* **207**, 119–134 (2015).
10. Giraldo, M. C. & Valent, B. Filamentous plant pathogen effectors in action. *Nat Rev Microbiol* **11**, 800–814 (2013).
11. Shang, S. *et al.* Fumarylacetoacetate hydrolase targeted by a *Fusarium graminearum* effector positively regulates wheat FHB resistance. *Nat Commun* **16**, 5582 (2025).
12. Cesari, S. Multiple strategies for pathogen perception by plant immune receptors. *New Phytologist* **219**, 17–24 (2018).
13. Kourelis, J. & van der Hoorn, R. A. L. Defended to the Nines: 25 Years of Resistance Gene Cloning Identifies Nine Mechanisms for R Protein Function. *Plant Cell* **30**, 285–299 (2018).
14. Wang, J. *et al.* Reconstitution and structure of a plant NLR resistosome conferring immunity. *Science* **364**, eaav5870 (2019).
15. Huang, S. *et al.* NLR signaling in plants: from resistosomes to second messengers. *Trends in Biochemical Sciences* **48**, 776–787 (2023).
16. Takken, F. L. & Goverse, A. How to build a pathogen detector: structural basis of NB-LRR function. *Current Opinion in Plant Biology* **15**, 375–384 (2012).
17. Tamborski, J. & Krasileva, K. V. Evolution of Plant NLRs: From Natural History to Precise Modifications. *Annu. Rev. Plant Biol.* **71**, 355–378 (2020).
18. Huang, S., Li, E., Jia, F., Han, Z. & Chai, J. Assembly and functional mechanisms of plant NLR resistosomes. *Current Opinion in Structural Biology* **90**, 102977 (2025).
19. Wang, J., Song, W. & Chai, J. Structure, biochemical function, and signaling mechanism of plant NLRs. *Molecular Plant* **16**, 75–95 (2023).

738 20. Jacob P. *et al*. Plant "helper" immune receptors are $Ca2^{+}$-permeable nonselective
739 cation channels. *Science* **373**, 420–425 (2021).
740 21. Wang, J. *et al.* Coordinated actions of NLR-assembled and glutamate receptor–like
741 calcium channels in plant effector-triggered immunity. *Proceedings of the National*
742 *Academy of Sciences* **122**, e2508018122 (2025).
743 22. Wang, J. *et al.* Plant NLR immune receptor Tm-22 activation requires NB-ARC
744 domain-mediated self-association of CC domain. *PLOS Pathogens* **16**, e1008475
745 (2020).
746 23. Baudin, M. *et al.* A natural diversity screen in *ARABIDOPSIS THALIANA* reveals
747 determinants for HopZ1a recognition in the ZAR1-ZED1 immune complex. *Plant Cell*
748 *& Environment* **44**, 629–644 (2021).
749 24. Kadota, Y. & Shirasu, K. The HSP90 complex of plants. *Biochimica et Biophysica*
750 *Acta (BBA) - Molecular Cell Research* **1823**, 689–697 (2012).
751 25. Shirasu, K. The HSP90-SGT1 Chaperone Complex for NLR Immune Sensors. *Annu.*
752 *Rev. Plant Biol.* **60**, 139–164 (2009).
753 26. Liu, Y., Burch-Smith, T., Schiff, M., Feng, S. & Dinesh-Kumar, S. P. Molecular
754 Chaperone Hsp90 Associates with Resistance Protein N and Its Signaling Proteins
755 SGT1 and Rar1 to Modulate an Innate Immune Response in Plants. *Journal of*
756 *Biological Chemistry* **279**, 2101–2108 (2004).
757 27. Zhang, Y., Dorey, S., Swiderski, M. & Jones, J. D. G. Expression of *RPS4* in tobacco
758 induces an AvrRps4-independent HR that requires EDS1, SGT1 and HSP90. *The Plant*
759 *Journal* **40**, 213–224 (2004).
760 28. Huang, S. *et al.* HSP 90s are required for NLR immune receptor accumulation in
761 Arabidopsis. *The Plant Journal* **79**, 427–439 (2014).
762 29. Holt BF 3rd, Belkhadir Y, Dangl JL. Antagonistic Control of Disease Resistance
763 Protein Stability in the Plant Immune System. *Science* **309**, 929–32 (2005).
764 30. Li, Y. *et al.* SRFR1 Negatively Regulates Plant NB-LRR Resistance Protein
765 Accumulation to Prevent Autoimmunity. *PLOS Pathogens* **6**, e1001111 (2010).
766 31. Yy, C., Hc, L., Ny, L., Fc, H. & Ss, K. *Arabidopsis* Hsa32, a novel heat shock protein,
767 is essential for acquired thermotolerance during long recovery after acclimation. *Plant*
768 *physiology* **140**, (2006).

769 32. Busch, W., Wunderlich, M. & Schöffl, F. Identification of novel heat shock factor-
770 dependent genes and biochemical pathways in *Arabidopsis thaliana*. *The Plant*
771 *Journal* **41**, 1–14 (2005).
772 33. Guo, X. *et al.* Heat-response patterns of the heat shock transcription factor family in
773 advanced development stages of wheat (*Triticum aestivum* L.) and thermotolerance-
774 regulation by TaHsfA2–10. *BMC Plant Biol* **20**, 364 (2020).
775 34. Ty, W. *et al.* Interplay between heat shock proteins HSP101 and HSA32 prolongs heat
776 acclimation memory posttranscriptionally in *Arabidopsis*. *Plant physiology* **161**,
777 (2013).
778 35. My, L. *et al.* A positive feedback loop between HEAT SHOCK PROTEIN101 and
779 HEAT STRESS-ASSOCIATED 32-KD PROTEIN modulates long-term acquired
780 thermotolerance illustrating diverse heat stress responses in rice varieties. *Plant*
781 *physiology* **164**, (2014).
782 36. Wang, X. *et al.* Massive expansion and differential evolution of small heat shock
783 proteins with wheat (*Triticum aestivum* L.) polyploidization. *Sci Rep* **7**, 2581 (2017).
784 37. Pradhan, G. P. & Prasad, P. V. V. Evaluation of Wheat Chromosome Translocation
785 Lines for High Temperature Stress Tolerance at Grain Filling Stage. *PLOS ONE* **10**,
786 e0116620 (2015).
787 38. Lu, P. *et al.* Landscape and regulation of alternative splicing and alternative
788 polyadenylation in a plant pathogenic fungus. *New Phytol* **235**: 674–689 (2022).
789 39. Fatima M, Anjum Bhat H, Rebekah N, Murugasamy S, Makandar R. Genome-wide
790 search and gene expression studies reveal candidate effectors with a role in
791 pathogenicity and virulence in *Fusarium graminearum*. *Mycologia* **116**: 708–728
792 (2024).
793 40. Kv, K., D, D. & Bj, S. Activation of an *Arabidopsis* resistance protein is specified by
794 the in planta association of its leucine-rich repeat domain with the cognate oomycete
795 effector. *The Plant cell* **22**, (2010).
796 41. Bernoux, M. *et al.* Structural and Functional Analysis of a Plant Resistance Protein
797 TIR Domain Reveals Interfaces for Self-Association, Signaling, and Autoregulation.
798 *Cell Host & Microbe* **9**, 200–211 (2011).

42. Maekawa, T., Kufer, T. A. & Schulze-Lefert, P. NLR functions in plant and animal immune systems: so far and yet so close. *Nat Immunol* **12**, 817–826 (2011).
43. Williams SJ. *et al*. Structural Basis for Assembly and Function of a Heterodimeric Plant Immune Receptor. *Science* **344**: 299-303 (2014).
44. Haslbeck, M., Weinkauf, S. & Buchner, J. Small heat shock proteins: Simplicity meets complexity. *Journal of Biological Chemistry* **294**, 2121–2132 (2019).
45. Haslbeck, M. & Vierling, E. A First Line of Stress Defense: Small Heat Shock Proteins and Their Function in Protein Homeostasis. *Journal of Molecular Biology* **427**, 1537–1548 (2015).
46. Bi, G. *et al.* The ZAR1 resistosome is a calcium-permeable channel triggering plant immune signaling. *Cell* **184**, 3528–3541.e12 (2021).
47. Förderer, A. *et al.* A wheat resistosome defines common principles of immune receptor channels. *Nature* **610**, 532–539 (2022).
48. Takken, F. L., Albrecht, M. & Tameling, W. I. Resistance proteins: molecular switches of plant defence. *Current Opinion in Plant Biology* **9**, 383–390 (2006).
49. Gou M, Shi Z, Zhu Y, Bao Z, Wang G, Hua J. The F-box protein CPR1/CPR30 negatively regulates R protein SNC1 accumulation. *Plant J* **69**: 411–20 (2012).
50. Yh, L. & Mp, M. Exploitation of the host cell ubiquitin machinery by microbial effector proteins. *Journal of cell science* **130**, (2017).
51. Wang, Z. *et al.* A Phytophthora infestans RXLR effector targets a potato ubiquitin-like domain-containing protein to inhibit the proteasome activity and hamper plant immunity. *New Phytol* **238**: 781–797 (2023).
52. Park, C. H. *et al.* The E3 Ligase APIP10 Connects the Effector AvrPiz-t to the NLR Receptor Piz-t in Rice. *PLOS Pathogens* **12**, e1005529 (2016).
53. Jx, L., G, L. & S, Ü. Selective autophagy: adding precision in plant immunity. *Essays in biochemistry* **66**, (2022).
54. Hubert, D. A. *et al.* Cytosolic HSP90 associates with and modulates the *Arabidopsis* RPM1 disease resistance protein. *EMBO J* **22**, 5679–5689 (2003).
55. Zheng, Z. *et al.* Atypical RXLR effectors are involved in *Phytophthora cactorum* pathogenesis. *aBIOTECH* **6**, 50 (2025).

56. Kadota, Y., Shirasu, K. & Guerois, R. NLR sensors meet at the SGT1–HSP90 crossroad. *Trends in Biochemical Sciences* **35**, 199–207 (2010).
57. Wu, Q. *et al.* The CC–NB–LRR protein BSR1 from Brachypodium confers resistance to Barley stripe mosaic virus in gramineous plants by recognising TGB1 movement protein. *New Phytol* **236**: 2233–2248 (2022).
58. Krasileva, K. V. *et al.* Uncovering hidden variation in polyploid wheat. *Proceedings of the National Academy of Sciences* **114**, E913–E921 (2017).
59. Wang, D. *et al.* Boosting wheat functional genomics via an indexed EMS mutant library of KN9204. *Plant Communications* **4**, 100593 (2023).
60. Jiang, C. *et al.* An expanded subfamily of G-protein-coupled receptor genes in *Fusarium graminearum* required for wheat infection. *Nat Microbiol* **4**, 1582–1591 (2019).
61. Wang, C. *et al.* Functional Analysis of the Kinome of the Wheat Scab Fungus *Fusarium graminearum*. *PLOS Pathogens* **7**, e1002460 (2011).
62. Jacobs, K. A. *et al.* A genetic selection for isolating cDNAs encoding secreted proteins. *Gene* **198**, 289–296 (1997).
63. Sk, O. *et al.* In planta expression screens of Phytophthora infestans RXLR effectors reveal diverse phenotypes, including activation of the *Solanum bulbocastanum* disease resistance protein Rpi-blb2. *The Plant cell* **21**, (2009).
64. Koschwanez, J. H., Foster, K. R. & Murray, A. W. Sucrose Utilization in Budding Yeast as a Model for the Origin of Undifferentiated Multicellularity. *PLOS Biology* **9**, e1001122 (2011).
65. D, D. *et al.* RXLR-mediated entry of *Phytophthora sojae* effector Avr1b into soybean cells does not require pathogen-encoded machinery. *The Plant cell* **20**, (2008).
66. Y, W. *et al.* OsHDAC1 deacetylates the aldehyde dehydrogenase OsALDH2B1, repressing OsGR3 and decreasing salt tolerance in rice. *Plant physiology* **198**, (2025).
67. Nielsen, H. Practical Applications of Language Models in Protein Sorting Prediction: SignalP 6.0, DeepLoc 2.1, and DeepLocPro 1.0. *Methods Mol Biol* **2941**: 153–175 (2025).
68. Jj, A. A. *et al.* Detecting sequence signals in targeting peptides using deep learning. *Life science alliance* **2**, (2019).

69. S, K., G, S. & K, T. MEGA7: Molecular Evolutionary Genetics Analysis Version 7.0 for Bigger Datasets. *Molecular biology and evolution* **33**, (2016).

Supplementary information

Supplementary Data 1. List of FgUP7 yeast screening libraries

Supplementary Data 1. List of TaRPM1 yeast screening libraries

Supplementary Data 3. Primers used in this study

Supplementary Fig. 1 Identification of putative candidate effectors from *F. graminearum.*

Supplementary Fig. 2 Confirmation of *F. graminearum* effector candidate (FgUP7) mutants and the plant basal defense gene expression.

Supplementary Fig. 3 Schematic representation of TaRPM1 protein domain architecture and FgUP7-mediated degradation of TaRPM1.

Supplementary Fig. 4 The KN9204 mutant of TaRPM1 confers susceptibility to *F. graminearum*.

Supplementary Fig. 5 Editing types and expression levels of *TaRPM1* transgenics.

Supplementary Fig. 6 Overexpression of *TaRPM1* has no significant effect on the agronomic traits of wheat.

Supplementary Fig. 7 TaRPM1 interacts with TaHSA32.

Supplementary Fig. 8 The N-terminus of TaRPM1-CC are required for interactions with TaHSA32.

Supplementary Fig. 9 Temperature induction of TaHSA32.

Supplementary Fig. 10 FgUP7 and TaHSA32 are co-localized.

Supplementary Fig. 11 BdRPM1 positively regulates *B. distachyon* resistance to *F. graminearum*.

Supplementary Fig. 12 BdRPM1 interacts with BdHSA32.

Figures and Legends

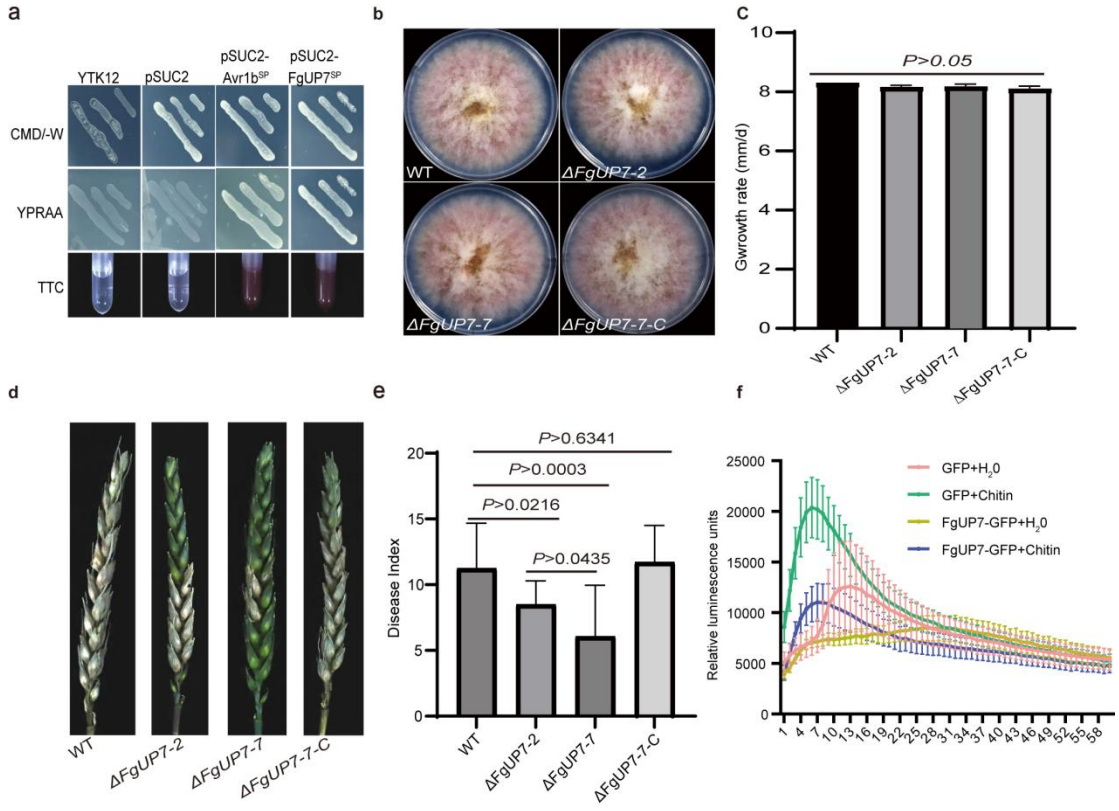

Fig. 1 FgUP7 is required for the pathogenicity of *F. graminearum* in wheat spikes.

(a) Functional validation of the FgUP7 signal peptide using the yeast invertase secretion assay. The YTK12 transformed yeast strain was able to grow on YPRAA medium with raffinose as the sole carbon source. The YTK12 strain with empty pSUC2 vector and the N-terminal sequence of *Phytophthora sojae* Avr1b were used as negative and positive controls, respectively.

(b) Colony morphology of the wild-type (WT), *ΔFgUP7* mutants (*ΔFgUP7*-2 and *ΔFgUP7*-7), and complemented strain (*ΔFgUP7*-7-C) after 5 days of cultivation on PDA plates.

(c) Bar graph showing the growth rates of the WT, *ΔFgUP7*-2, *ΔFgUP7*-7, and *ΔFgUP7*-7-C strains. Data represent three biological replicates.

(d) Disease symptoms on wheat spikes at 14 days post-inoculation with the WT, *ΔFgUP7*-2, *ΔFgUP7*-7, and *ΔFgUP7*-7-C strains.

(e) Distribution of disease indices on wheat caused by the WT, *ΔFgUP7*-2, *ΔFgUP7*-7, and *ΔFgUP7*-7-C strains.

(f) The chitin-induced ROS accumulation in *N. benthamiana* leaves expressing GFP or *FgUP7*-GFP. Data were obtained from 12 biologically independent samples.

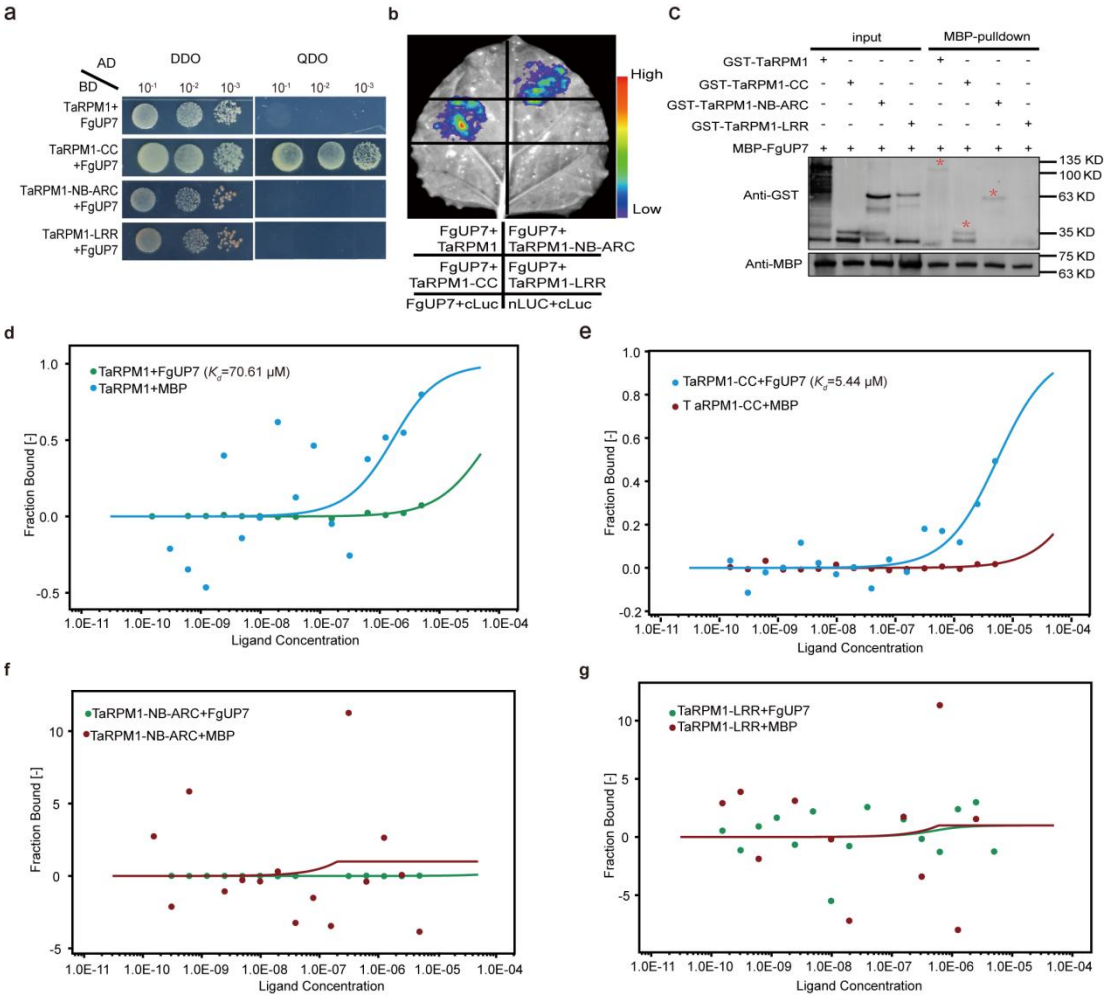

Fig. 2 FgUP7 interacts with TaRPM1.

(a) Yeast two-hybrid assay showing the interaction between FgUP7 and the TaRPM1-CC domain. Transformants were grown on DDO (SD/-Trp/-Leu) and QDO (SD/-Trp/-Leu/-His/-Ade) media.

(b) LCI assay in *N. benthamiana* leaves. Leaves were co-infiltrated with *A. tumefaciens* (GV3101) carrying FgUP7-cLuc paired with TaRPM1-nLuc, TaRPM1-CC-nLuc, TaRPM1-NB-ARC-nLuc, or TaRPM1-LRR-nLuc. Luminescence signals were captured 72 hours post-infiltration.

(c) Pull-down analysis of the interactions between FgUP7 and full-length TaRPM1, TaRPM1-CC, TaRPM1-NB-ARC, and TaRPM1-LRR. GST-tagged TaRPM1, TaRPM1-CC, TaRPM1-NB-ARC, and TaRPM1-LRR proteins were immunoprecipitated using

MBP-FgUP7 immobilized on MBP–agarose beads. Input and precipitated proteins were detected using anti–GST and anti–MBP antibodies. Red asterisk indicates the band corresponding to the protein of interest, if multiplebands were observed.

(d-g) MST was employed to evaluate the binding capacity of FgUP7 with TaRPM1 **(d)** and TaRPM1-CC **(e)**, TaRPM1-NB-ARC **(f)**, TaRPM1-LRR **(g)**. Ten-micrometer MBP–FgUP7 or empty-MBP was labeled by RED–NHS. The raw data were integrated and fitted to a binding model using the MST analysis software. The recombinant proteins were contained in NT standard capillaries. The solid curve is the fit of the data points to the standard *Kd*-fit function. *Kd*, dissociation constant.

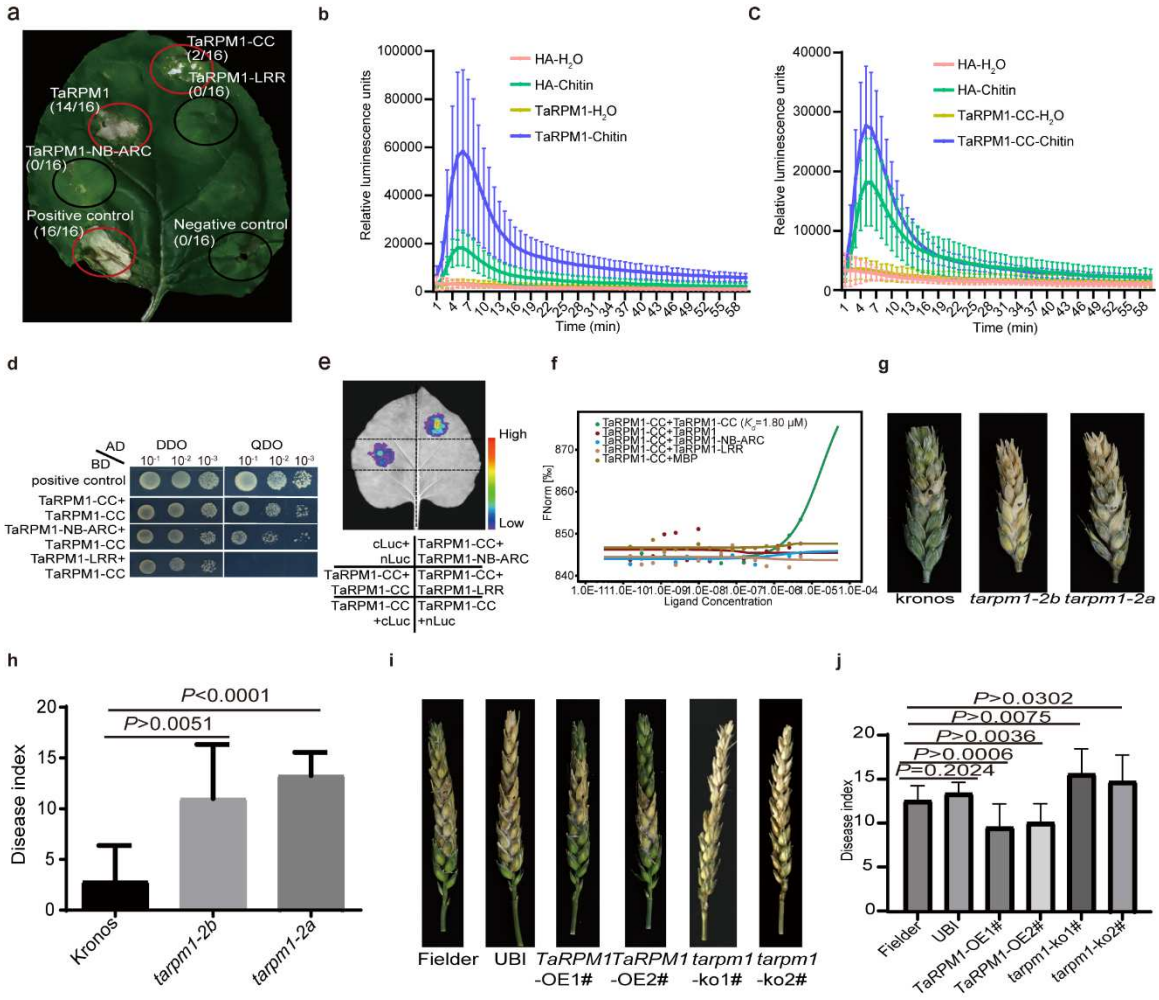

Fig. 3 The TaRPM1-CC domain self-associates and TaRPM1 positively regulates resistance against *F. graminearum*.

(a) Full-length TaRPM1 and its truncated variants (TaRPM1-CC, TaRPM1-NB-ARC, and TaRPM1-LRR) were expressed as GFP fusions to assess their ability to trigger cell death in *N. benthamiana*. Green fluorescent protein (GFP) and BAX were used as negative and positive controls, respectively. Sixteen leaves were examined per construct. The percentage of leaves displaying a hypersensitive response (HR) is shown. Data represent three independent biological replicates.

(b-c) TaRPM1 **(b)** and TaRPM1-CC **(c)** suppress chitin-induced reactive oxygen species (ROS) burst in *N. benthamiana* leaves.

(d) Yeast two-hybrid assay showing self-interaction of TaRPM1 and TaRPM1-CC.

(e) LCI assay confirming self-interaction of TaRPM1 and TaRPM1-CC in *N.*

benthamiana.

(f) MST analysis of the binding affinity between TaRPM1-CC and TaRPM1, TaRPM1-CC, TaRPM1-NB-ARC, or TaRPM1-LRR. RED–NHS–labeled MBP–TaRPM1-CC (10 μM) or MBP alone (control) was used. Raw MST data were processed and fitted with the standard dissociation constant (*Kd*) model. Recombinant proteins were loaded into standard-treated capillaries, and the solid line represents the curve fit of the data points. *Kd*, dissociation constant.

(g) Disease symptoms on *kronos* mutant wheat spikes at 14 days post inoculation (dpi) with wild-type *F. graminearum*.

(h) Distribution of disease indices in *kronos* mutant plants inoculated with wild-type *F. graminearum* at 14 dpi. Data are from three independent experiments.

(i) Disease symptoms on wheat cultivar Fielder overexpressing or gene-edited for *TaRPM1* at 14 dpi with wild-type *F. graminearum*.

(j) Distribution of disease indices in Fielder wheat lines overexpressing or gene–edited for *TaRPM1* at 14 dpi. Data are from three independent experiments.

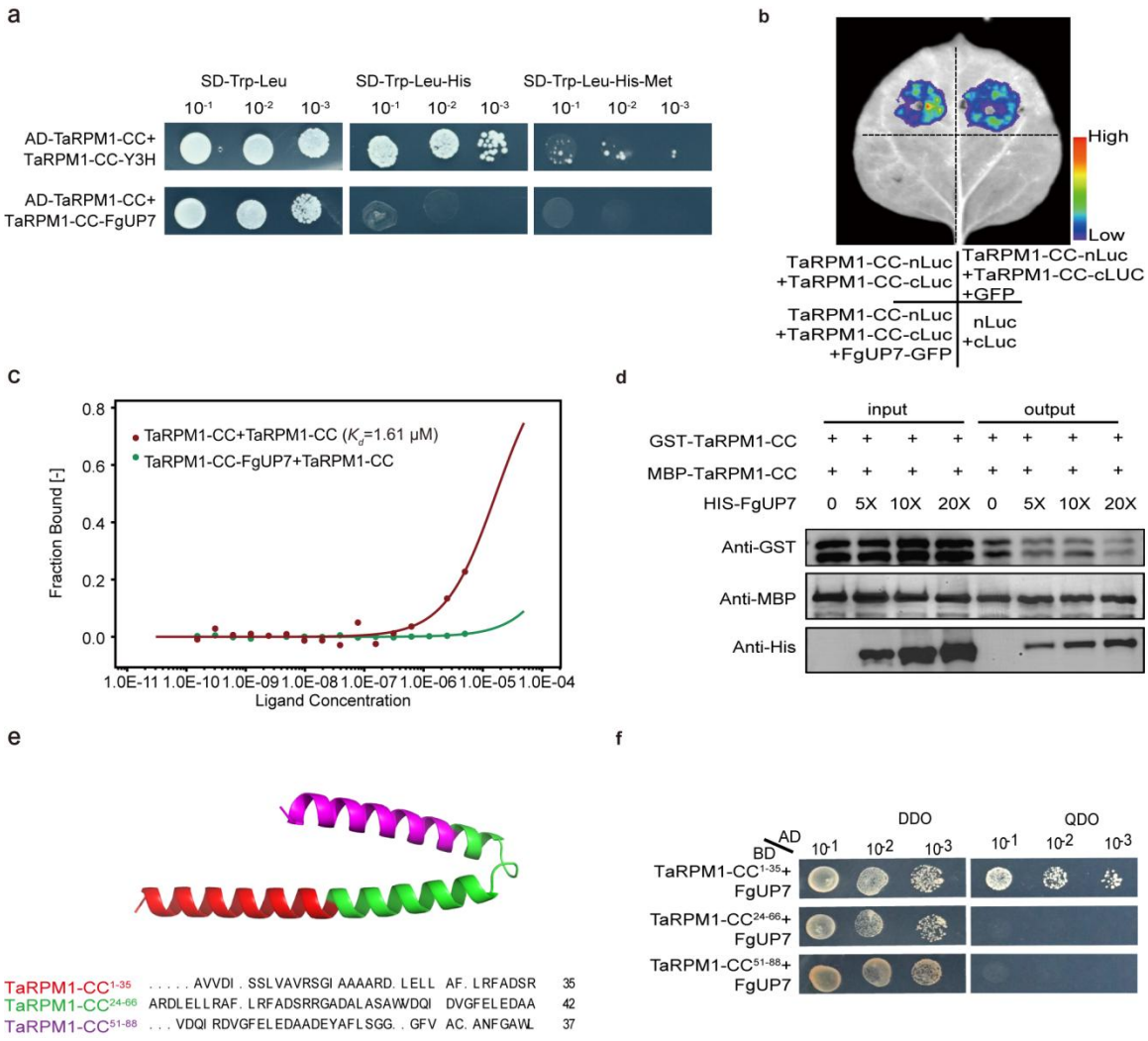

Fig. 4 FgUP7 Targets the N-Terminal Region of the TaRPM1 CC Domain to Disrupt CC Self-Interaction.

(a) Yeast three-hybrid assay was performed to assess TaRPM1-CC self-interaction in the presence or absence of FgUP7. Growth assays on SD medium lacking Trp, Leu, and His (-TLH), or Trp, Leu, His, and Met (-TLHM), showed that FgUP7 inhibited TaRPM1-CC self-interaction under both conditions. An unlabeled TaRPM1-CC construct was used as a control.

(b) LCI assay comparing the interaction between TaRPM1-CC and itself when co-expressed with or without FgUP7.

(c) MST was used to evaluate the effect of FgUP7 on TaRPM1-CC self-binding affinity. The solid line represents the curve fit of the data points to a standard *Kd*-fitting function. *Kd*, dissociation constant.

(d) Pull-down assay examining the influence of FgUP7 on the interaction between GST-TaRPM1-CC and MBP-TaRPM1-CC. Proteins were incubated with increasing concentrations of HIS-FgUP7. The complexes were pulled down using MBP agarose magnetic beads coupled with MBP-TaRPM1-CC, and detected with anti-GST, anti-MBP, and anti-HIS antibodies. The experiment was repeated twice with similar results.

(e) Schematic of structures of TaRPM1-CC mutants.

(f) Interaction assays of FgUP7 with TaRPM1-CC mutants in yeast. Transformants were grown on DDO (SD/-Trp/-Leu) and QDO (SD/-Trp/-Leu/-His/-Ade) media.

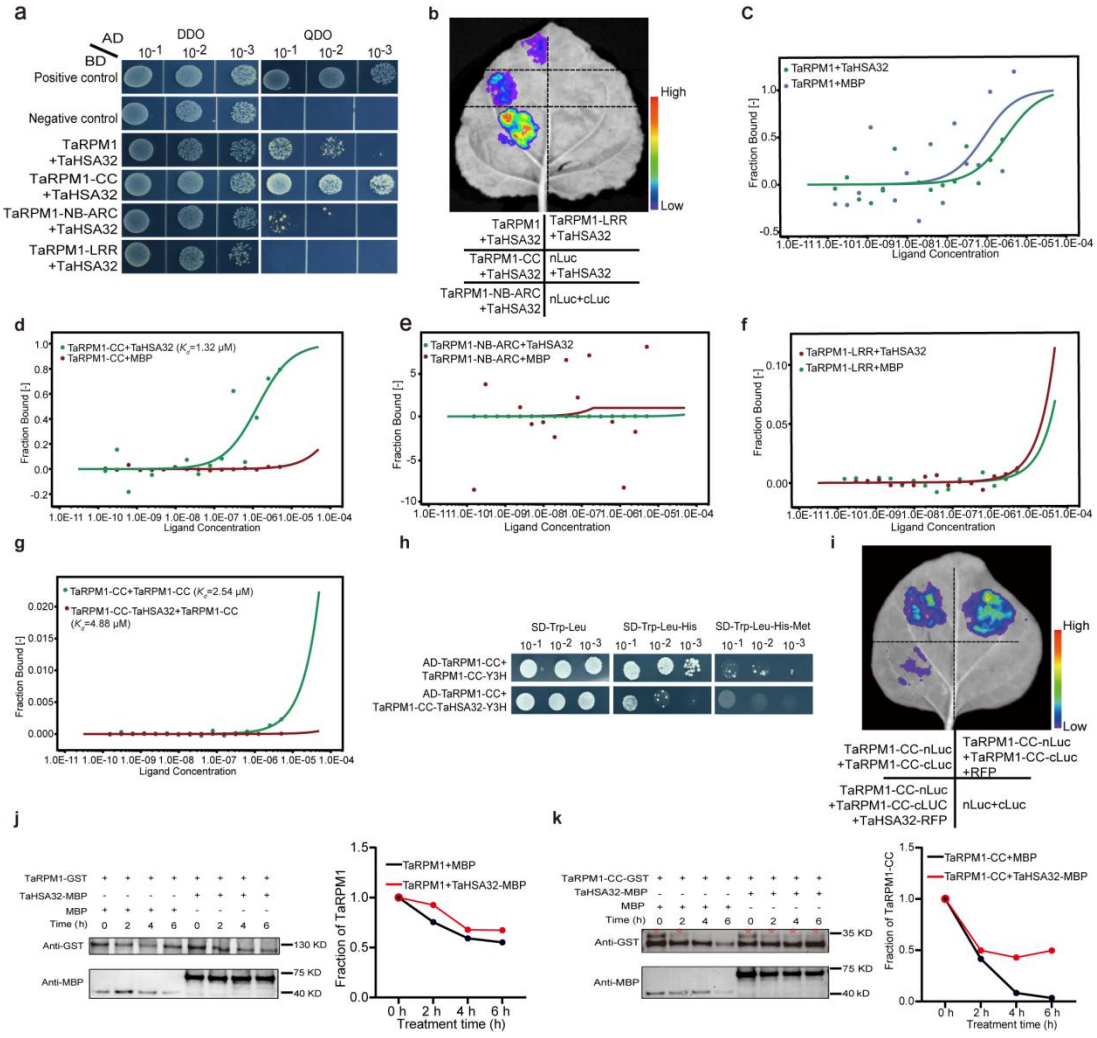

Fig. 5 TaRPM1 interacts with TaHSA32, and TaHSA32 stabilizes the TaRPM1.

(a-b) Interaction between TaHSA32 and TaRPM1, TaRPM1-CC, or TaRPM1-NB-ARC was detected by yeast two-hybrid assay **(a)** and LCI assay **(b)**.

(c-f) Binding affinity of TaHSA32 to TaRPM1 **(c)**, TaRPM1-CC **(d)**, TaRPM1-NB-ARC **(e)**, and TaRPM1-LRR **(f)** measured by MST. Recombinant, purified TaRPM1, TaRPM1-CC, TaRPM1-NB-ARC, TaRPM1-LRR protein was labeled with a fluorescent dye, while TaHSA32 and MBP proteins were used as mobile analytes in a MST assay. Raw data were processed and fitted to a binding model using MST analysis software. Recombinant proteins were loaded into standard treated capillaries. The solid curve represents the fit of the data points to the standard *Kd* fitting function. *Kd*, dissociation constant.

(g) MST was used to evaluate the effect of TaHSA32 on TaRPM1-CC self-binding affinity. The solid line represents the curve fit of the data points to a standard *Kd*–fitting function. *Kd*, dissociation constant.

(h) Yeast three-hybrid assay was performed to assess TaRPM1-CC self-interaction in the presence or absence of TaHSA32. Growth assays on SD medium lacking Trp, Leu, and His (-TLH), or Trp, Leu, His, and Met (-TLHM), showed that TaHSA32 inhibited TaRPM1-CC self-interaction under both conditions. An unlabeled TaRPM1-CC construct was used as a control.

(i) LCI assay comparing the interaction between TaRPM1-CC and itself when co-expressed with or without TaHSA32.

(j-k) In vitro co-incubation assays evaluating the effect of TaHSA32 on the stability of TaRPM1 and its truncated proteins. GST-TaRPM1 **(j)** or GST-TaRPM1-CC **(k)** was incubated at 37°C for 0, 2, 4, and 6 hours. Protein levels were detected using anti-GST and anti-MBP antibodies.

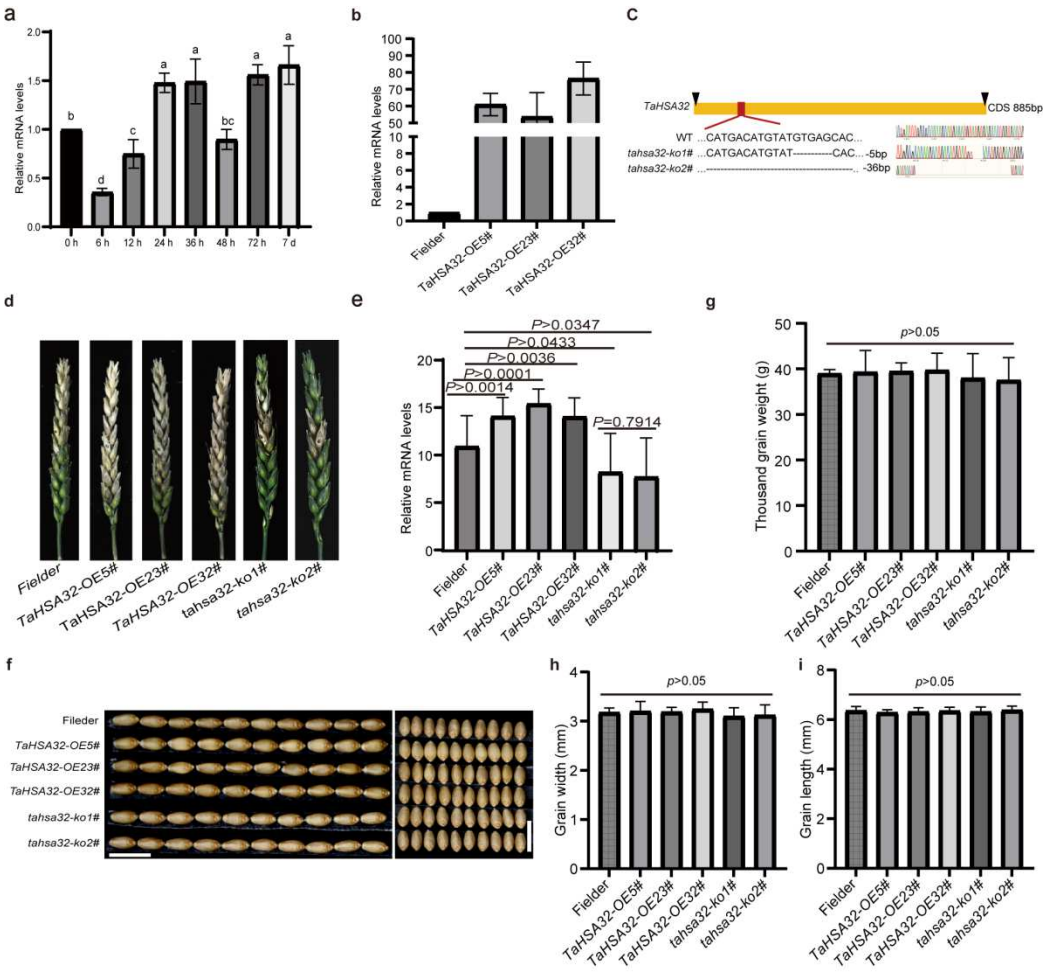

Fig. 6 TaHSA32 negatively regulates wheat resistance to *F. graminearum*, and transgenic lines with *TaHSA32* overexpression or knockout exhibit no detectable changes in agronomic traits.

(a) RT–qPCR analysis of *TaHSA32* expression induced by *F. graminearum* infection. Spike samples of the wheat cultivar Fielder collected at 0 hours post-inoculation were set as 1. *TaActin* was used as the internal reference gene. Data are from three biological replicates.

(b) Expression level analysis of T1 generation *TaHSA32* overexpression lines.

(c) Genotypic identification of *TaHSA32* CRISPR/Cas9-edited lines.

(d) Disease symptoms on spikes of Fielder wheat (overexpressing or gene-edited for *TaHSA32*) at 14 days post-inoculation with the wild-type *F. graminearum* strain.

(e) Distribution of disease indices in Fielder wheat (overexpressing or gene-edited for *TaHSA32*) at 14 days post-inoculation. Data are from three independent experiments. **f)** Seed morphology of Fielder, *TaHSA32*-OE, and *TaHSA32*-KO plants at grain maturity stage. Scale bar: 1 cm.

(g-i) Thousand-kernel weight **(g)**, kernel length **(h)**, and kernel width **(i)** of Fielder, *TaHSA32*-OE, and *TaHSA32*-KO plants. Values represent the mean ± SD from at least three independent experiments. All data were analyzed by one-way ANOVA compared with the wild-type Fielder plants.

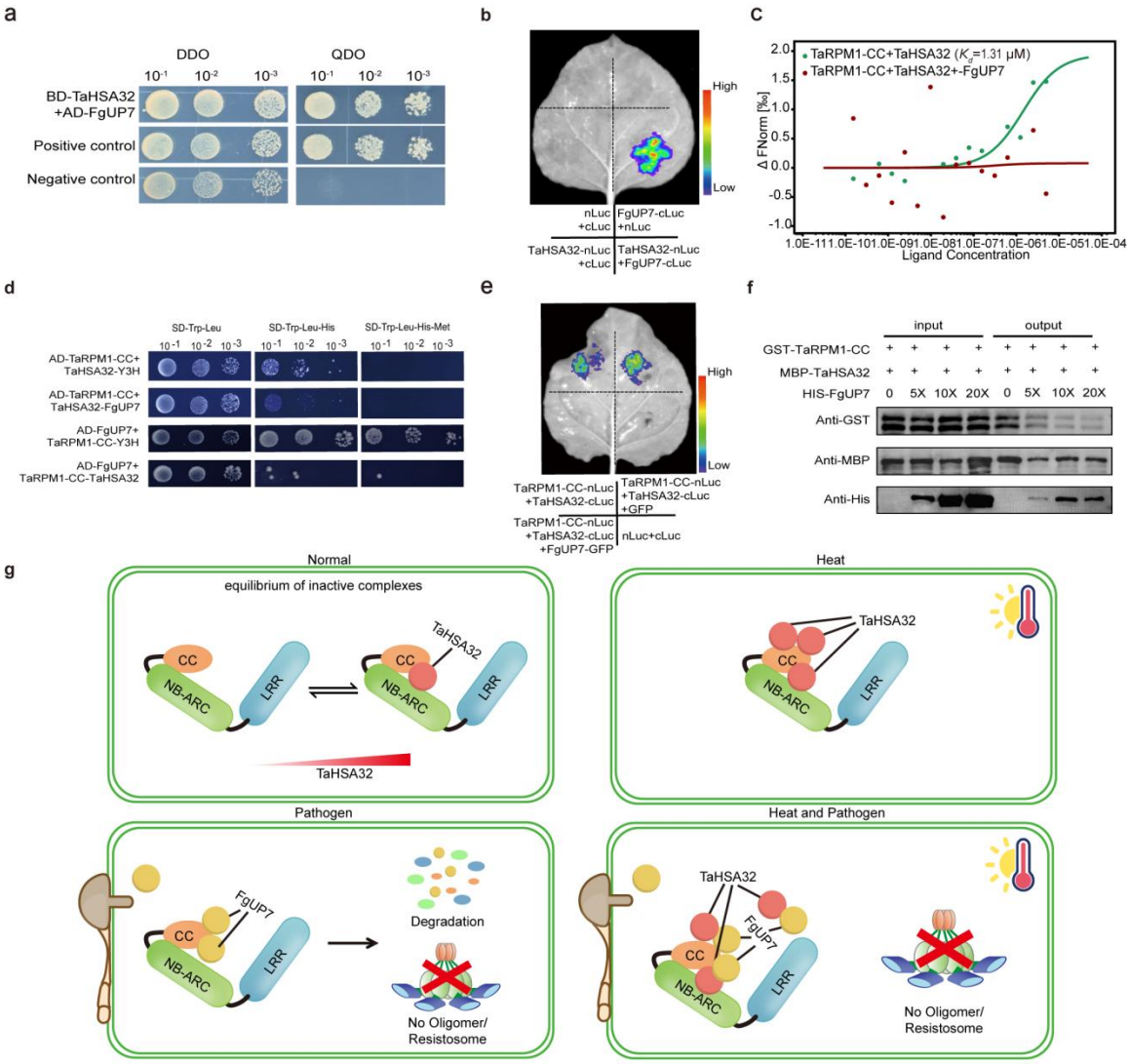

1018

1019 **Fig. 7 FgUP7 suppresses both TaRPM1-CC self-interaction and its interaction with**
1020 **TaHSA32.**

1021 **(a)** Yeast two-hybrid assay showing the interaction between FgUP7 and the TaHSA32.
1022 Transformants were grown on DDO (SD/-Trp/-Leu) and QDO (SD/-Trp/-Leu/-His/-Ade)
1023 media.

1024 **(b)** LCI assay in *N. benthamiana* leaves. Leaves were co-infiltrated with *A. tumefaciens*
1025 (GV3101) carrying FgUP7-cLuc paired with TaHSA32-nLuc. Luminescence signals were
1026 captured 72 hours post-infiltration.

(c) MST analysis of the binding affinity between TaRPM1-CC and TaHSA32 in the presence of FgUP7. The solid line represents the fitted binding curve, and *Kd* indicates the dissociation constant.

(d-f) Yeast three-hybrid **(d),** LCI **(e)** and pull-down **(f)** assays were conducted to analyze TaRPM1-CC–TaHSA32 interaction with or without FgUP7. The experiment was repeated twice with similar results.

(g) The proposed working model of FgUP7–TaRPM1–TaHSA32. Under normal conditions, TaRPM1 exists in equilibrium between inactive complexes with or without TaHSA32, which binds the CC domain and maintains basal NLR stability. Heat stress induces TaHSA32, which acts as a molecular chaperone to stabilize TaRPM1. During pathogen infection, the *Fusarium* effector FgUP7 targets the N-terminal CC domain, disrupting CC self-interaction and early oligomerization while promoting full-length TaRPM1 degradation, reducing immune surveillance. Under combined heat and pathogen stress, FgUP7 competitively binds TaHSA32, destabilizing the TaRPM1–HSA32 molecular lock and further inhibiting NLR activation.

Supplementary Files

This is a list of supplementary files associated with this preprint. Click to download.

- SupplementaryFigure.pdf
- SupplementaryInformationfiles.xlsx